



**Photonanomedicine: A Convergence of Photodynamic Therapy and Nanotechnology**

Journal:	<i>Nanoscale</i>
Manuscript ID	NR-REV-12-2015-008691.R2
Article Type:	Review Article
Date Submitted by the Author:	01-Jun-2016
Complete List of Authors:	Obaid, Girgis; Wellman Center for Photomedicine, Dermatology Broekgaarden, Mans; Wellman Center for Photomedicine, Dermatology Bulin, Anne-Laure; Wellman Center for Photomedicine, Dermatology Huang, Huang-Chiao; Wellman Center for Photomedicine, Dermatology Kuriakose, Jerrin; Wellman Center for Photomedicine, Dermatology Liu, Joyce; Wellman Center for Photomedicine, Dermatology Hasan, Tayyaba; Massachusetts General Hospital and Harvard Medical School, Wellman Center for Photomedicine

Abbreviation	Definition
$^1\text{O}_2$	Singlet oxygen
$^3\text{O}_2$	Triplet oxygen
ABC	ATP-binding cassette (transporters)
ALA	5-aminolevulinic acid
AMD	Age-related macular degeneration
AML	Acute myeloid leukemia
BPD	Benzoporphyrin derivative
Ce6	Chlorin e6
CELSI	Cerenkov-excited luminescence-scanned imaging
Cet	Cetuximab
CMA	Chlorin e6-monoethylenediamine monoamide
CT	Computed Tomography
DMSO	Dimethylsulfoxide
DPPC	1,2-dipalmitoyl- <i>sn</i> -glycero-3-phosphocholine
DPPG	1,2-dipalmitoyl- <i>sn</i> -glycero-3-phospho-(1'- <i>rac</i> -glycerol)
DPSE-PEG	1,2-distearoyl- <i>sn</i> -glycero-3-phosphoethanolamine- <i>N</i> -(polyethylene glycol)
EGFR	Epidermal growth factor receptor
EMA	European Medicines Agency
EPC	Egg phosphatidylcholine
EPR	Enhanced permeability and retention (effect)
ER	Endoplasmic reticulum
Fab	Fragment antigen binding
FDA	Food and Drug Administration
GLP	Good Laboratory Practice
GMP	Good Manufacturing Practice
iCCD	Intensified charge-coupled device
ICG	Indocyanine green
IR	Infrared
MRI	Magnetic resonance imaging
MSN	Mesoporous silica nanoparticle
mTHPC	Meta-tetra (hydroxyphenyl)chlorin
nanoPAL	Nanophotoactivatable liposome
NCP	Nanoscale coordination polymer
NIR	Near-infrared
NP	Nanoporphyrin
NSCLC	Non-small cell lung cancer
OvCa	Ovarian carcinoma
PAI	Photoacoustic imaging
PD	Pharmacodynamics
PCI	Photochemical internalization
PDT	Photodynamic therapy
PEG	Polyethylene glycol
PET	Positron emission tomography
PIC	Photoimmunoconjugate
PIT	Photoimmunotherapy
PLG	poly(DL-lactide/glycolide)
PLGA	poly(lactide-co-glycolic acid)
PMIL	Photoactivatable multi-inhibitor nanoliposome
PNM	Photonanomedicine
PpIX	Protoporphyrin IX
PS	Photosensitizer

PTT	Photothermal therapy
RES	Reticuloendothelial system
RFA	Radiofrequency ablation
RMS	Reactive molecular species
RT	Radiation therapy
SDA	Single domain antibody
SERS	Surface-enhance Raman spectroscopy
taPIT	Tumor-targeted activatable photoimmunotherapy
TiO <sub>2</sub>	Titanium dioxide
UV	Ultraviolet
VEGF	Vascular endothelial growth factor
vPDT	Vascular photodynamic therapy
XL184	Cabozantinib, Cometriq®
ZnPC	Zinc phthalocyanine

## Photonanomedicine: A Convergence of Photodynamic Therapy and Nanotechnology

Girgis Obaid, Mans Broekgaarden,\* Anne-Laure Bulin,\* Huang-Chiao Huang,\* Jerrin Kuriakose,\* Joyce Liu\* and Tayyaba Hasan<sup>a,b</sup>

\*Authors with equal contributions

<sup>a</sup>Harvard Medical School, Wellman Center for Photomedicine, Massachusetts General Hospital, Boston, Massachusetts, USA. <sup>b</sup>Harvard-MIT Division of Health Science and Technology, Boston, Massachusetts, USA.

Correspondence should be addressed to Tayyaba Hasan ([thasan@mgh.harvard.edu](mailto:thasan@mgh.harvard.edu))

### Abstract

As clinical nanomedicine has emerged over the past two decades, phototherapeutic advancements using nanotechnology have also evolved and impacted disease management. Because of unique features attributable to the light activation process of molecules, photonanomedicine (PNM) holds significant promise as a personalized, image-guided therapeutic approach for cancer and non-cancer pathologies. The convergence of advanced photochemical therapies such as photodynamic therapy (PDT) and imaging modalities with sophisticated nanotechnologies is enabling the ongoing evolution of fundamental PNM formulations, such as Visudyne<sup>®</sup>, into progressive forward-looking platforms that integrate theranostics (therapeutics and diagnostics), molecular selectivity, the spatiotemporally controlled release of synergistic therapeutics, along with regulated, sustained drug dosing. Considering that the envisioned goal of these integrated platforms is proving to be realistic, this review will discuss how PNM has evolved over the years as a preclinical and clinical amalgamation of nanotechnology with PDT. The encouraging investigations that emphasize the potent synergy between photochemistry and nanotherapeutics, in addition to the growing realization of the value of these multi-faceted theranostic nanoplatforms, will assist in driving PNM formulations into mainstream oncological clinical practice as a necessary tool in the medical armamentarium.

### Introduction - The evolution of photonanomedicine

Over the past two decades, nanotechnology has experienced a rapid diversification in its potential applications. Starting out as a pure physical and materials science study of nanoscale crystalline and composite materials, the realization that nanotechnology could spearhead new approaches to overcome hurdles in pharmaceuticals and in clinical disease management, paved the way for a new era of research into medical nanotechnology: nanomedicine. In many ways, the eagerly-anticipated clinical impact of nanomedicine has been somewhat delayed by the increasing evidence that some materials, as attractive as their utility might be, exert complex effects on the body. Research into improving the clinical translatability of nanomedicines has branched into multiple new avenues of exploration, where a selection of the vast existing pool of nanomaterials are fine-tuned to improve biocompatibility, tolerance and physiological efficacy. This capacity for precise alterations of the nanomaterial composition and the respective surface properties is one of the main attractions of exploring their use as novel medicines. From a chemical standpoint, the macromolecular and supramolecular modification of nanomaterials and their precursors is evolving as a new complementary perspective to more traditional synthetic chemistry approaches for small molecule therapeutics development. The explosion in peer-reviewed publications and patents reporting novel nanomaterials proposed for specific niches within the clinic serves as a direct illustration of the collective opinion held by many researchers that nanomedicine can address multiple longstanding unmet clinical needs.

According to the European Patent Office, there are 55,830 patents filed globally to date that relate to nanoparticle technologies, in addition to the 16,908 patents filed covering liposomal technologies.<sup>1</sup> Globally, there are a total of 209 ongoing and completed clinical trials using nanoparticles for various applications in oncology, ophthalmology, dental medicine and infectious disease, amongst numerous others.<sup>2</sup> Of those, 82 are ongoing and only 3% have been withdrawn prior to enrollment due to funding limitations and poor patient recruitment. Moreover, there are

1,641 ongoing and completed clinical trials globally using liposomes, a clinically-accepted class of nanosized drug delivery vehicles that simultaneously encapsulate hydrophilic and lipophilic agents.<sup>3,4</sup> Figure 1 shows the global demographic of the five largest contributors to clinical trials of both nanoparticles and liposomes to date.

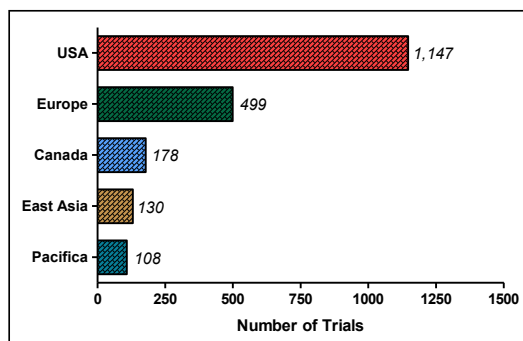


**Figure 1.** Distribution of the total number of clinical trials using nanoparticles and liposomes in the five highest contributing regions of the world.<sup>5</sup>

Into this mix of innovative approaches to nanomedicine has emerged photonanomedicine (PNM), which incorporates light-activatable entities in nanomaterials with potential for exquisite spatiotemporal control. This review will discuss the progress, hurdles and prospects of PNM formulations in clinical cancer diagnostics and medicine. A specific emphasis will be placed on one of the most widely explored, photochemistry-driven process in PNM, photodynamic therapy (PDT).<sup>6,7</sup> PDT is based on the energy-specific activation of visible and near-infrared (NIR) absorbing molecules, photosensitizers (PSs), to generate reactive molecular species (RMS) that are phototoxic to the target disease tissues, as shown in Figure 2 (A).

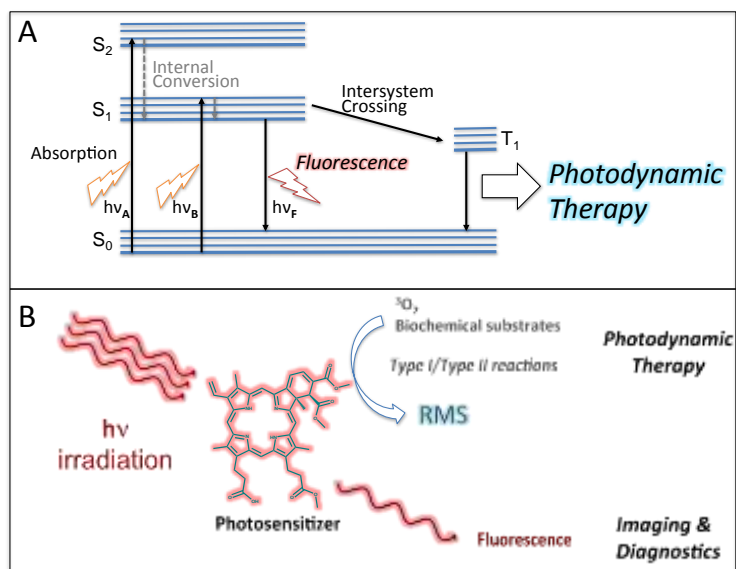


**Figure 2. A)** A schematic representation of the Jablonski diagram showing how PDT and fluorescence induced is by the irradiation of a PS. The PS in the ground state ( $S_0$ ) becomes excited by incident light ( $h\nu_A$  or  $h\nu_B$ ) to the  $S_1$  or  $S_2$  singlet excited states. The excited PS can relax to  $S_0$  by the radiative fluorescence emission of photons ( $h\nu_F$ ), which can be used for imaging and diagnostics, or can undergo a spin forbidden process termed intersystem crossing. Through the spin flip of the excited PS, the molecule occupies a long-lived triplet excited state ( $T_1$ ), from which photochemical reactions occur that result in the production of cytotoxic RMS, including  $^1O_2$ , that is used for PDT. **B)** A diagrammatic representation of the use of a PS for PDT and imaging techniques. Through type I and type II photochemical reactions, the excited sensitizer generates cytotoxic  $^1O_2$  and RMS from ground state triplet oxygen ( $^3O_2$ ) and various biochemical substrates. The concomitant fluorescence of the PSs allows for imaging and diagnostic uses, emphasizing their inherent theranostic capacity.

The generation of various therapeutic RMS molecules proceeds through two distinct, yet interchangeable photochemical processes: type I reactions that produce radicals and radical ions, and oxygen-dependent type II reactions that produce singlet oxygen ( $^1O_2$ ) and oxygen radicals. Both photochemical reactions are initiated from the triplet excited state of the PS; however, radiative relaxation processes of photoexcited PSs give rise to fluorescent (singlet excited to singlet ground state relaxation) and phosphorescent (triplet excited state to singlet ground state relaxation) emission of light. Owing to their fluorescent properties, PSs are inherently therapeutic and diagnostic (theranostic) agents. Figure 2 (B) is a visual representation of the theranostic nature of PS molecules, where photoexcitation results in type I and type II reactions for PDT, whilst concurrently resulting in fluorescence emission that is used for a variety of imaging and diagnostic applications. Although still largely investigational, PNM was an early player in the field of nanomedicine. Visudyne<sup>®</sup>, a non-PEGylated liposomal formulation of the PS benzoporphyrin derivative (BPD), was one of the early nanotherapeutics to be approved by the U.S. Food and Drug Administration (FDA) as a first line treatment of age-related macular degeneration (AMD) and is considered an instrumental paradigm of photoactive nanotherapeutics and nanodiagnostics.<sup>8</sup> Clinically, PDT is performed through the administration of a PS or its respective formulation, followed by the timely irradiation of the disease tissue using NIR light that optimally penetrates tissue in wavelength range known as the 'optical window' ranging between 600 nm and 1300 nm.<sup>9</sup> The most effective PSs are those that have been tuned to maximally absorb NIR light within that optical window. Figure 3 is a graphical summary of clinical PDT and describes the different PS formulations that will be discussed in this review in addition to the functional and structural imaging modalities used in conjunction.

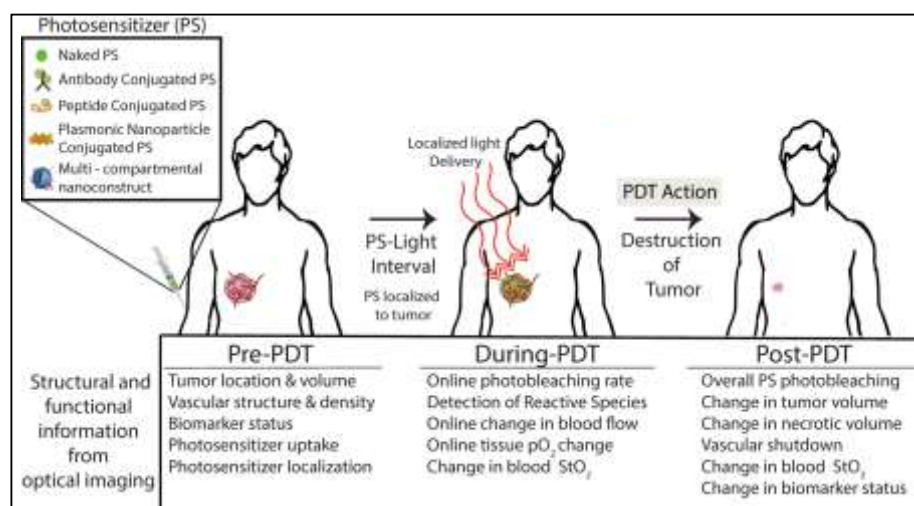


**Figure 3.** A representation of the steps taken during a clinical PDT procedure using various PS formulations and the structural and functional information obtained using optical imaging techniques that enables treatment prediction and guidance. Following intravenous administration of the PS, an appropriate PS-light interval is required prior to irradiation using localized NIR light delivery. Through spatially confined PDT action on the tumor, the disease tissue is destroyed. Figure adapted with permission from Mallidi *et al.*<sup>10</sup> Optical Imaging, Photodynamic Therapy and Optically Triggered Combination Treatments, *The Cancer Journal*, 21 (3), p194-205. (Copyright © 2015 Wolters Kluwer Health, Inc.)

The importance of the photoactivity of nanotherapeutics is not only restricted to their use in phototherapies, but also encompasses multiple parameters that distinguish such PNM formulations from the emerging pool of therapeutics. PNM formulations provide spatiotemporal control in the induction of phototherapy, spatial confinement in the phototriggered release of secondary encapsulated complementary therapeutics, temporal regulation of their respective activity and the combination of multiple theranostic agents that can be hyperspectrally and spatiotemporally resolved. This review will outline recent advancements in PNM formulations developed with respect to imaging-assisted, and rationally designed anti-cancer combination regimens. Efforts

from our laboratories and others are universally driven towards achieving a unifying therapeutic and diagnostic (theranostic) nanoparticle represented in Figure 4.

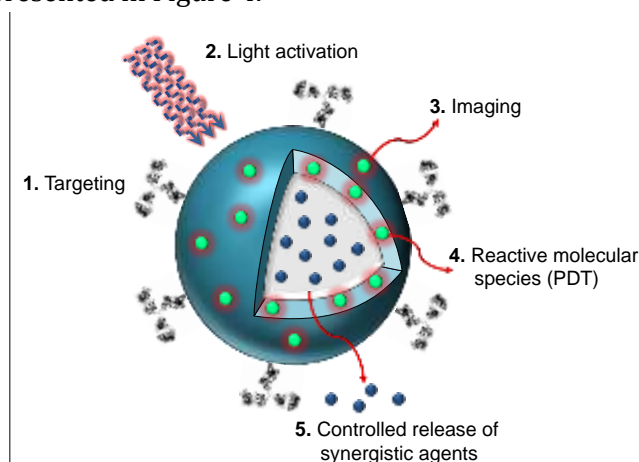


**Figure 4.** A schematic diagram of the visionary theranostic nanoconstruct that combines a fluorescence-based theranostic or imaging agent and a therapeutic drug encapsulated within. The surface is grafted with a targeting ligand to enable the molecular selectivity of the theranostic PNM formulation (1). Light activation using NIR light can be used for image-guided therapy (2), photochemical generation of cytotoxic RMS for PDT of the disease tissue (4) and sequential, controlled release of synergistic agents for combinatorial cancer therapy (5).

The envisioned nanoconstruct realizes 1) the capacity to molecularly target tumors 2) the ability to mediate optical diagnostics and dosimetry 3) the selective induction of photodynamic action and 4) the spatiotemporal control of phototriggered release of synergistic anti-neoplastic agents. Progression driving technology closer to this visionary nanoconstruct will be highlighted in this review.

The fluorescence properties of PSs are highly effective for a variety of applications that distinguish them from conventional anti-cancer drugs that are formulated as nanomedicines. These include the potential for fluorescence pharmacokinetic (PK) quantitation of tumor PS concentrations,<sup>11</sup> the fluorescence guidance of surgical tumor resection<sup>12</sup> and the online monitoring of PDT dosimetry parameters through rates of PS photobleaching.<sup>13-15</sup> The preclinical and clinical applications of multi-faceted theranostic PSs and the successive forward-looking PNM formulations will be discussed in greater detail in the *Theranostics* section.

Phototherapeutics are by no means restricted to the photochemistry-based PDT. Other noteworthy modalities exist and are emerging in clinical trials. Though not focused on in this review, photothermal therapy (PTT) plays a role in nanomedicine, such as plasmonic gold nanostructures.<sup>16,17</sup> There are currently two active clinical trials using plasmonic gold nanoshells, AuroShell®, for anti-cancer PTT specifically termed AuroLase® Therapy.<sup>18,19</sup> Requiring significantly higher power densities ( $\text{W}/\text{cm}^2$ ) than PDT ( $\text{mW}/\text{cm}^2$ ), the therapeutic response times for PTT ranging in the  $10^{-3}$  – 1 s timeframe are significantly shorter than those of PDT (1 -  $10^3$  s).<sup>20</sup> Power densities for PDT and PTT can oftentimes overlap when photothermal agents are utilized as mediators for PPT. However, considerable higher concentrations of photothermal agents are required for tissue thermalization with lower power densities, as compared to PDT. PDT is an attractive option when prolonged agent interaction times and a precise spatiotemporal controlled drug release is required. Unlike PTT, an attribute of PDT is the excellent healing process of normal tissue, thus scarring and collateral damage is minimized. The threshold nature of the PDT process also allows for the PS to be present in non-target sites as long as the overall PDT dose can be below the threshold for damage.<sup>21</sup> This enables the illumination of larger volumes of tissue to ensure tumor margin sterilization. Ultimately, a selection of phototherapeutic strategies with distinct modes of action can be employed to address specific clinical needs.

## Clinical nanomedicine

### Past, present and future

The improved outcomes from many of the now-approved nanotechnology-based therapeutics have encouraged a sustained clinical effort, with several trials ongoing or recently completed. While the clinical advancements discussed here are by no means comprehensive, they will touch on some of the most recent results that highlight the varied capabilities offered by nanotechnology. A specific focus will be made on the nanomedicines requiring additional activation or triggered release, which can be selectively localized to the disease site. Figure 5 is a relatively comprehensive timeline outlining some of these liposomes, polymer and protein-based nanomedicines that have been approved by the FDA and other regional official medical regulatory bodies. The major driving force for the initial nanoformulations of the listed drugs was the improvement in their PK profiles and tolerability upon encapsulation. The developments of advanced nanomedicines to follow were motivated by a number of needs that were unmet by conventional nanoformulations. These include the need for increased control over activity and spatiotemporal drug release, the necessity for selectivity in targeted delivery of agents and the significance of multi-agent co-encapsulation. Highlights and technological advances in the global clinical progression of these multi-faceted 'soft' nanoformulations will be described in this section.

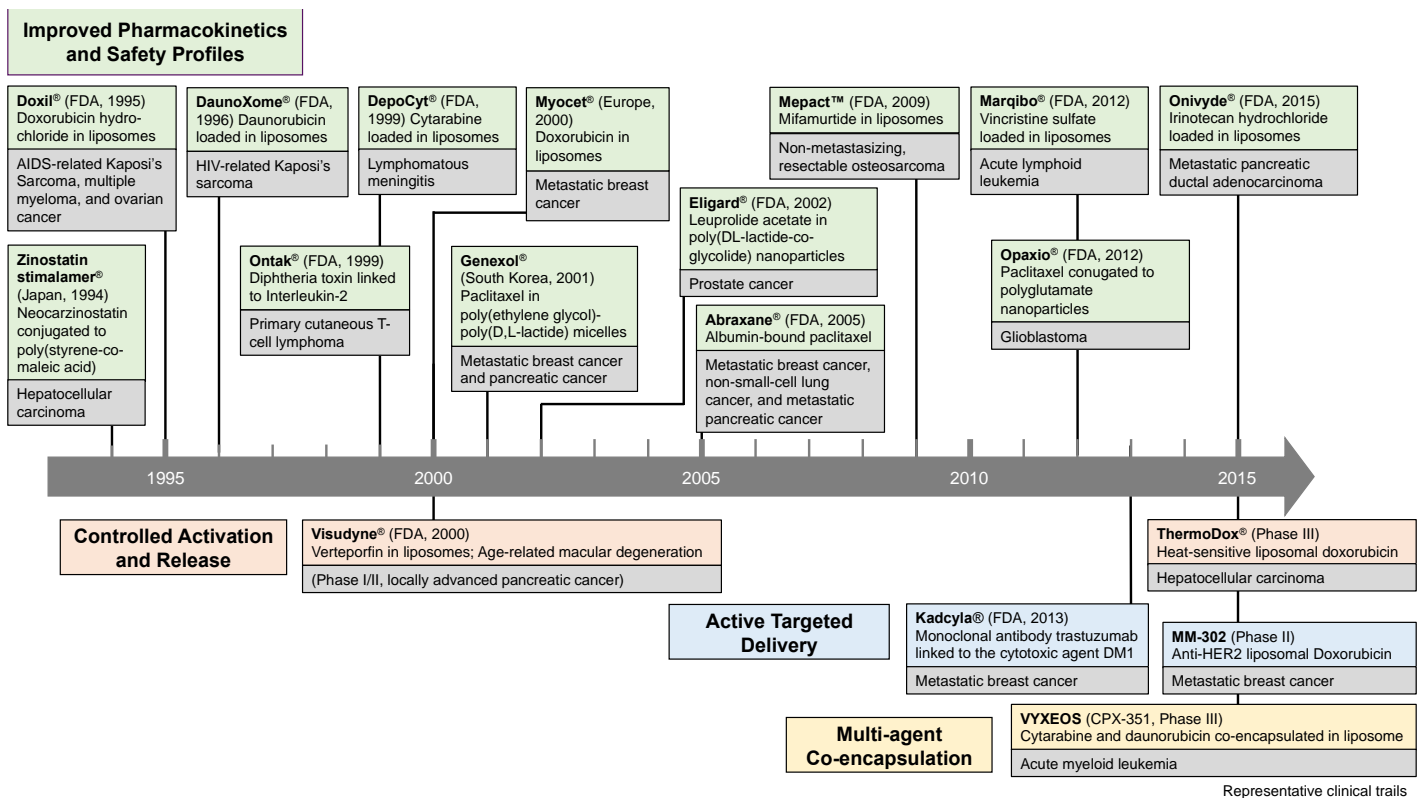


**Figure 5.** A timeline spanning the late 1990's to date listing the chronological approval and clinical trial status of some lipid, polymer, and protein-based anti-cancer nanomedicines that are being leveraged to improve the PKs, safety profiles, and therapeutic indices of anti-neoplastic agents. The nanomedicines are classified under subgroups that describe the nature and primary utility of the clinical nanomedicines listed. These include nanomedicines that serve to improve drug PKs and safety profiles, to enable the controlled activation and release of therapeutics, to actively target and selectively deliver agents and those that act as a platform for multi-agent co-encapsulation. Visudyne®, which gained approval in 2000, is currently the only soft PNM formulation which enables controlled light activation. Controlled photoactivation of Visudyne® using 690 nm NIR light was approved for PDT of AMD, and Visudyne®-PDT is now showing significant promising in clinical trails for locally advanced pancreatic cancers.<sup>22</sup>

In the last quarter of a century, approximately 100 nanomedicine products have been introduced to the market for therapeutic or medical device applications.<sup>23</sup> One of the most noticeable advancements has been in the field of oncology using soft organic nanoconstructs, such as liposomes, micelles, and polymeric and protein-based nanoparticles.<sup>24</sup> The majority of these commercialized nanomedicine products are developed for intravenous

injection, taking advantage of the size- and shape-dependent enhanced permeability and retention (EPR) effect in tumor vasculature for 'passive targeting' of solid tumors. More recently, significant clinical efforts have been made to develop targeted nanomedicine that can be activated by external stimuli, such as light, or even administered orally, which is preferred by most patients.<sup>25</sup> Nevertheless, all these nanotechnologies have provided a solution to many hurdles in drug delivery, such as poor drug solubility and stability, suboptimal PK profiles and adverse systemic side-effects, all of which will be discussed in further detail within this review.

In the context of PNM, in 2000, the FDA approved the non-PEGylated liposomal BPD formulation, Visudyne®, for the PDT management of the wet form of AMD. To date, PDT using Visudyne® has saved the vision of millions of patients with retinal pathologies, and has been shown to work even more effectively using combination strategies.<sup>26</sup> As discussed earlier, the liposomal PNM formulation Visudyne® pushes the boundaries of typical nanotherapeutics in that it enables the regulation of spatiotemporal control over treatment induction, and thus bears huge clinical potential with regards to the impact this regulated approach can have on combination cancer therapies.<sup>8, 27</sup> The immediate clinical impact of Visudyne® is further evidenced in the ongoing clinical trials for pancreatic cancers.<sup>22</sup> In our VERTPAC-01 Phase I/II trial, PDT was conducted using Visudyne® in patients with locally advanced pancreatic cancer.<sup>22</sup> Laser light at 690 nm can be delivered *via* single or multiple fibers positioned percutaneously under computed tomography (CT) guidance for photochemical activation of Visudyne® within the tumor interstitium. At 40J, PDT consistently induced 12 mm of necrosis in the tumors with a low incidence of mild adverse events (*e.g.* abdominal pain and inflammation), thus meeting all endpoints of the study. In the same trial, CT scans prior to and following treatment showed a strong positive correlation between contrast-derived venous blood content and necrotic volume in the tumor.<sup>28</sup> These results suggested that contrast CT could provide key surrogate dosimetry information to assess treatment response and will be discussed further in the *Theranostics* section. In an earlier clinical study on patients with locally advanced pancreatic cancer, Bown *et al.* performed PDT using the PS meso-tetrahydroxyphenyl chlorin (mTHPC), that is reconstituted in a mixture of water and ethanol containing polyethylene glycol (PEG).<sup>29</sup> In this study, up to six optical fibers were used to deliver light percutaneously under CT guidance for effective mTHPC- PDT, which had a remarkable 100% response rate and a median overall survival of 9.5 months. More recently, Moore *et al.* demonstrated that the PS WST-11, a Cremophor® emulsion of the palladium-bacteriopheophorbide TOOKAD®, can be used for ultrasonography-guided vascular-targeted PDT of low-risk prostate cancer in patients that have limited therapeutic intervention options.<sup>30</sup> It should be noted that the delivery of light can be achieved in many ways and, in the case of pancreatic cancer discussed above, ultrasound guided endoscopes and fiber optics also provide a conduit for direct light delivery into deep situated tumors. Placement of multiple fibers is also possible for treating large tumors such as glioblastoma.<sup>22, 31</sup> To manage tumors with poorly defined margins or those of disseminated nature, light delivery over large areas is made possible clinically with diffusing tip fibers, balloons and scattering media.<sup>32</sup>

To put the growing excitement of the emerging oncological indications of PNM formulations into perspective, the current clinical status of soft nanotechnology that are often used in the building blocks of advanced PNM formulations will be reviewed. Selective tumoral activation of nanotechnology is also being clinically evaluated with Celsion™'s ThermoDox® in the Phase III HEAT trial for hepatocellular carcinoma.<sup>33</sup> ThermoDox® is a PEGylated liposomal formulation designed to thermally release doxorubicin upon radiofrequency ablation (RFA). Results made available from Celsion™'s press releases indicate that an extended duration of RFA may be critical to improving outcomes, leading to the initiation of a new Phase III trial, OPTIMA, for hepatocellular carcinoma.<sup>34-36</sup>

Although not part of PNM, Doxil®, a liposomal formulation of doxorubicin must be mentioned in any discussion of nanomedicine, as it was the first liposomal drug to be approved by the FDA in 1995.<sup>3</sup> Doxil® is approved for the treatment of various cancers including AIDS-related Kaposi's sarcoma, recurrent OvCa and multiple myeloma.<sup>3</sup> A major feature of Doxil® is the presence of surface PEG molecules that provide the liposomes with a stealth quality. 'PEGylation' protects the inner encapsulating doxorubicin from the external environment, prolongs circulation time to enhance passive tumor drug accumulation, and reduces cardiotoxicity associated with doxorubicin therapy. A more recent advancement in clinical nanomedicine is the FDA approval of Onivyde® (MM-398, nal-IRI), a

liposomal formulation of irinotecan.<sup>37, 38</sup> Approval for gemcitabine-refractory pancreatic cancer in 2015 was granted after the Phase III NAPOLI-1 study demonstrated an improved median overall survival using Onivyde® in combination with 5-fluorouracil and leucovorin.<sup>37, 38</sup> Besides adding new functionality to existing FDA-approved small molecule chemotherapeutics, liposomal nanotechnology also extends to the delivery of vaccines and of PSs for cancer treatments.<sup>39</sup>

Analogous to liposomes, polymer and protein-based nanotherapeutics have also been used to improve the PK and toxicity profiles of common potent chemotherapeutics. NKTR-102 is another nanoformulation of irinotecan made by Nektar Therapeutics™, which consists of a polymeric nanoparticle conjugated to the drug. NKTR-102 is currently in Phase I to III trials for a variety of indications.<sup>40-43</sup> Data from the Phase III BEACON trial with NKTR-102 thus far indicates that only breast cancer patient subgroups with brain and liver metastases show a significant overall survival benefit.<sup>44, 45</sup> Genexol®, a PEG-poly (lactic acid) micellar formulation of paclitaxel with a diameter of ~20-50 nm, was approved for use in South Korea in patients with metastatic breast and pancreatic cancers in 2001.<sup>46</sup> Eligard® is a poly(DL-lactide/glycolide) (PLG) nanoparticle incorporating leuprolide acetate, which was approved in 2002 for advanced prostate cancer.<sup>47</sup> Abraxane® is an albumin-bound paclitaxel nanoparticle, ~130 nm in diameter, which was approved by the FDA in 2005 for passive targeting of metastatic breast cancer and was approved by the European Medicines Agency (EMA) for the same disease in 2008. Abraxane® received FDA approval for the treatment of locally advanced or metastatic non-small cell lung cancer (NSCLC) in 2012, which was shortly followed by approval for the treatment of metastatic adenocarcinoma of the pancreas by the FDA and EMA in 2013.<sup>48</sup>

Beyond these capabilities, nanoscale complexes, such as liposomes and/or nanoparticles, can also be leveraged for the co-encapsulation of multiple therapeutic agents, which may be mechanistically desirable. These advances in nanoformulations allow the delivery of fixed-ratio drug combinations with unified PKs, along with the option for drug compartmentalization to regulate sequential release kinetics. Furthermore, the potential for cancer targeting and light-triggered drug release may further improve treatment outcomes in cancer. Co-encapsulated nanoformulations of dual agents are already showing promise in human trials. For example, liposomally co-encapsulated cytarabine and daunorubicin (CPX-351, Celator Pharmaceuticals™), recently completed testing in Phase II studies for acute myeloid leukemia (AML).<sup>49</sup> CPX-351 showed a significantly improved response rate and overall survival from 4.2 to 6.6 months in patients with secondary AML, when compared to patients treated with the standard combination of free cytarabine and daunorubicin.<sup>50</sup> Preclinically, our group recently developed a photoactivatable multi-compartmental nanoconstruct that contains a 'membrane-like' unilamellar liposomal shell for the loading of the PS BPD and a PEG-poly (lactic-co-glycolic acid) (PLGA) nanoparticle core containing an anti-angiogenic agent.<sup>51</sup> The anti-angiogenic agent is photo-released within the tumor to synergistically reduce both local tumor burden and distant metastases of pancreatic cancer *in vivo*.<sup>51</sup> Leveraging the hydrophobic and hydrophilic compartments of folate-targeted liposomes, Morton *et al.* effectively co-encapsulated both hydrophobic (erlotinib) and hydrophilic (doxorubicin) therapeutics to enhance A459 tumor control *in vivo* via the dynamic rewiring of apoptotic signaling pathways.<sup>52</sup>

Clinical advances have also been made in actively targeted, bioconjugated nanoformulations. Epidermal growth factor receptor (EGFR)-targeted immunoliposomes encapsulating doxorubicin were the earliest targeted chemotherapeutic immunoliposome in clinical trials, demonstrating potent antitumor activity in Phase I studies.<sup>53</sup> Merrimack Pharmaceuticals™ has also developed a human epidermal growth factor receptor-2 (HER-2) targeted doxorubicin immunoliposome, MM-302, for the treatment of breast cancer, which is currently in Phase II trials.<sup>55</sup> BIND Therapeutics™ has also developed BIND-014, a docetaxel PEG-PLGA polymeric nanoparticle targeting prostate specific membrane antigen, which is currently in Phase II trials for prostate cancer and non-small cell lung carcinoma.<sup>56</sup> This nanoconstruct is currently being initiated for an even broader range of indications. These examples of nanotherapeutics, amongst many others emerging for a large variety of oncological and non-oncological indications, demonstrate not only the clinical enthusiasm of nanomedicine and PNM but also pave the

way for using light-activated, targeted, and combinatorial approaches that improve current drugs previously limited in their efficacy and safety.

### Challenges to the clinical translation of photonanomedicine.

As discussed in this review, incorporating the PDT approach with nanotechnology allows for the encapsulation of high PS payloads, improved photoactivity and appropriately-timed release and activation of therapeutic agents. As with all parenteral non-PDT nanoconstructs, understanding pharmacokinetics (PKs) of advanced nanoformulations and their respective constituents is fundamental in maximizing their therapeutic efficacy and expediting clinical translation. Each constituent exhibits individually unique PK and toxicology profiles, in addition to different metabolic and physiological clearance mechanisms. Furthermore, their cohesive behavior as an individual entity is distinctly different, as the resultant nanoformulation is essentially a new material. *In vivo* destabilization and degradation, therefore, results in complex multi-parametric physiological behaviors for each constituent of the nanoformulation. In addition to chemical composition, physical properties of nanoformulations govern the degree of efficacy and toxicity. For example, a 75 nm variant of Doxil<sup>®</sup>, was compared to the standard 100 nm formulation and was found to be more efficacious yet more toxic in tumor-bearing mice.<sup>57</sup> By incorporating PS into nanoformulations, PDT using PNM formulations has its own challenges. Whilst one of the advantages that we have mentioned in the body of the manuscript is that light can act as a drug release mechanism, with that comes another challenge in the need for studying new PK parameters of the released drugs. However, despite this additional layer of complexity, preclinical evidence of the efficacy of anti-cancer PNM formulations has been very promising.

Unlike nanoformulations of small molecule therapeutics, encapsulated into a nanoconstruct, the physiological effects of advanced PNM formulations are not only restricted to the agent and the nanocarrier properties. PDT with PNM formulations involves the paired use of an administered agent or multiple agents formulated into one or more nanoconstructs, that is activated by an applied optical irradiation. Thus, the clinical approval of PNM formulations is dependent on the regulation of the PS, the secondary therapeutic agents when applicable, the nanomaterials used for their formulation and the light sources for photoactivation. As a result of complex tissue light scattering and attenuation events, NIR light penetration through vascularized soft tissue is limited to approximately 1 cm, thereby necessitating the use of secondary medical devices for the procedure, namely optical fibers.<sup>22, 58, 59</sup> Optical fibers deliver light to deeply situated tumors, overcoming the limitation of light penetration, yet providing an additional regulatory obstacle in the approval of clinical PDT procedures. Clinically, the advances in fiber optic light conduits and image-guided approaches have empowered the applications of PDT that use an interstitial fiber placed directly within deep tumors. Placement of multiple fibers is also possible when treating large tumors, such as pancreatic tumors.<sup>22</sup> For diffuse carcinomas with poorly defined margins, such as disseminated ovarian cancer metastases, light delivery over the large peritoneal cavity surface areas is made possible clinically with diffusing tip fibers, balloons and scattering media.<sup>60</sup> In principle, the approval of novel PNM formulations can be expedited by the use of pre-approved and clinically approved PSs,<sup>61, 62</sup> biocompatible nanomaterials,<sup>63, 64</sup> targeted biologics,<sup>65, 66</sup> light sources,<sup>62, 67</sup> optical fibers<sup>68</sup> and imaging modalities to guide therapy.<sup>69</sup> Nonetheless, clinical approval of complex PNM formulations is still a big challenge because each individual formulation will become a different material and full screening becomes critical following any modification.

For the most part, downstream manufacture and quality control processes of the constituents comprising the evolving pre-clinical soft PNM formulations discussed in this review are well established in the biopharmaceutical industry. These constituents include liposomes, soft nanoparticles, photoactive nanoformulations and antibody-drug conjugates. Although amalgamations and modifications of the existing PNM formulation constituents will inevitably impact PK/pharmacodynamics (PD), toxicology and efficacy, the existing industrial infrastructure for Good Manufacturing Practice (GMP) scale-up synthesis of these advanced PNM formulations will facilitate and support their Good Laboratory Practice (GLP) toxicology studies and clinical trials. As mentioned in the previous

section, one of the early PNM formulations to be approved in the clinic is Visudyne® and, therefore, there is much optimism for more complex constructs to enter into the clinic.

Forward-looking preclinical advances in inorganic PNM formulations, such as nanoscintillators<sup>70</sup> and upconversion nanoparticles<sup>71</sup> have enabled the conversion of deep-penetrating radiation, such as X-rays and NIR light, to visible wavelengths for deep-tissue PS excitation. However, these ambitious nanomaterials are hindered by the inherent toxicity of their components and dopants, such as heavy metal ions and rare-earth lanthanide ions. Before being considered for clinical human use, rigorous *in vivo* toxicology, chemical stability, physiological integrity and clearance studies are crucial to confirm their safety. Furthermore, there must be a clear clinical advantage of using such nanomaterials over more conventional direct visible and NIR-mediated PDT agents.

Despite the fact that PDT has been shown to induce distant antitumor immunity in various animal models, clinical PDT is primarily used to manage local tumors. Numerous preclinical studies have shown that PDT sensitizes tumors to inhibition by systemic cytotoxic therapies, thus reducing the spread of disease to other sites indirectly when used in combination.<sup>51, 72</sup> Therefore, it is believed that PDT is best combined with systemic treatment modalities to maximize both local and distant tumor control. The combination of localized PDT and systemically cytotoxic therapies is also attractive for cancer treatment, which avoids overlapping toxicities and reduces the doses required to achieve the same therapeutic effect. Infrequent undesirable secondary reactions to PDT comprise skin burning, itching, and injection site reactions that include pain, edema, inflammation, extravasation, rashes, hemorrhage, and discoloration.<sup>22, 73</sup> Although most adverse events reported with PDT were of short duration and easily manageable, it is often critical for patients to avoid direct sunlight for 24-48 hours after treatment, depending on the skin clearance rates of the PS and its respective formulation. In contrast to PDT, most chemotherapies and biologics are associated with significant and long-term side effects, such as neutropenia, diarrhea and hair-loss, and patients often require dose reduction or preemptive management. The genotoxicity of DNA-damaging cancer therapies like alkylating agents and radiation therapy is not observed with PDT, as the lack of nuclear localization of most PS molecules confines oxidative damage to the target perinuclear organelles. Unlike external beam radiation, PDT can also be repeated several times at the same site if needed, given that PS selectivity to the tumor is optimal. Moreover, studies have suggested that PDT-induced damage is generally more efficient in the tumor than tissue, thus reducing normal tissue toxicity, regardless of PS selectivity.<sup>29</sup> Reasons for this are unclear, but elevated levels of reactive oxygen species scavengers in normal tissue are suggested.<sup>29, 74</sup>

It is becoming increasingly evident that conventional, uninformed PDT using free PSs may not be the most effective choice for cancer management. More sophisticated formulations, combination therapies, irradiation procedures and image-guidance needed to improve the clinical outcome of PDT will also impact the financial costs of the therapy. As with all other treatment modalities, additional pathological factors, such as completeness of response and the need for multiple rounds of therapy, can also influence the total costs. In general, a comprehensive treatment for pre-skin cancers may cost up to \$3,500 USD for a series of treatments, and can often be covered by health insurance in the United States.<sup>75</sup> Clinical applications of imaging-assisted PDT can be more precise, effective and less invasive, yet will lead to higher overall treatment costs. For example, clinical endoscopic PDT for early esophageal cancer can cost up to ~\$5,000 (USD), which is somewhat higher than the costs of chemoradiotherapy, radiofrequency ablation and cryoablation therapy, which ranges from \$1,500 to \$3,700 USD. However, compared to standard esophagectomy that costs more than \$25,000 USD, endoscopic PDT is considerably more cost-effective, and has a lower mortality rate with fewer major side effects.<sup>75</sup>

### **Theranostics**

The concept of combining therapeutics with diagnostics is encompassed in the fairly well-known term, *theranostics*. PDT is inherently a theranostic modality as the molecules involved are both photochemically active (to achieve the therapeutic effect) and fluorescent (to achieve the diagnostic component). Because of the differences in treatment response observed between *in vitro* and *in vivo* systems and because of the high variability among patients that receive the same treatment, the 'one size fits all' approach for PDT is not appropriate.<sup>76</sup> Thus,

there is growing interest for developing personalized medicine and adapting the treatment in real time. This personalized medicine is a common goal of all these theranostic applications. Particular to PDT, several strategies may be employed to reach this objective: 1) individualize PDT dosimetry by monitoring PS fluorescence, 2) use the PS fluorescence properties to guide surgery, and 3) monitor the treatment efficiency by involving other imaging modalities, such as CT, magnetic resonance imaging (MRI) or photoacoustic imaging (PAI).

### Optically- guided theranostics

As mentioned in the introduction, once a PS is photoexcited, it can relax either through intersystem crossing transitions eventually leading to the generation of cytotoxic RMS molecules, or by fluorescence emission that is concurrently exploited for optical imaging. Both pathways are exploited to assess PDT efficiency and perform dosimetry measurements: the singlet oxygen ( $^1O_2$ ) generation and the photobleaching of fluorescence of the PS.

#### **a. PS fluorescence and singlet oxygen measurements as dosimetry parameters**

Both photodestruction of the PS (photobleaching) during the PDT process and the quantitation of  $^1O_2$  have been proposed as means for patient-customization of PDT dosimetry. Using *in vitro* experiments performed on AML5 leukemic cells undergoing PDT using 5-aminolevulinic acid (ALA), Niedre *et al.* demonstrated in 2003 that cell survival was directly correlated with the phosphorescence intensity of  $^1O_2$  emitted at 1270 nm.<sup>77</sup> As a consequence, measuring the intensity of the infrared (IR) emission of  $^1O_2$  in real-time is a direct way of monitoring PDT efficiency and may even aid in predicting treatment outcomes. The  $^1O_2$  IR emission is weak and requires sophisticated imaging infrastructures; therefore, dynamic longitudinal monitoring of  $^1O_2$  generation is particularly challenging in the clinic. A more realistic method of clinically assessing the degree of  $^1O_2$  generation, and thus treatment response, is the dynamic monitoring of PS photobleaching. All PS molecules are subject to varying degrees of photobleaching directly through self-oxidation following irradiation. Jarvi *et al.* proposed in 2012 an *in vitro* comparative study investigating two dose metrics: the  $^1O_2$  emission metric, then considered as a gold-standard metric, and the metric for photobleaching of the PS.<sup>14</sup> They demonstrated that a positive linear correlation exists between the administered  $^1O_2$  dose calculated from the phosphorescence counts of  $^1O_2$  relaxation and PS photobleaching measurements. However, they also established that the survival rate is only correlated with the degree of photobleaching as long as the oxygen partial pressure remains above 5  $\mu$ M. Thus, photobleaching is not a reliable parameter for PDT under hypoxia. In 2014, Mallidi *et al.* published a clinical comparison between the two metrics on 26 healthy patients subjected to ALA-PDT.<sup>78</sup> The study showed a stronger positive correlation between evolution of erythema (PDT tissue sensitization) and the PS photobleaching induced by PDT than with the  $^1O_2$  phosphorescence emission. With the evolution of better detection systems and imaging modalities, the possibility of monitoring both direct (photobleaching metrics and  $^1O_2$  phosphorescence) and indirect (structural and functional properties of the tumor) treatment prediction parameters will drive the theranostics arena towards patient personalization. Towards this goal, the following sections discuss the current developments in imaging techniques and nanotechnology geared towards personalized therapies using integrated PNM formulations.

#### **b. Advances in imaging and spectroscopy**

Outstanding progress has been made from the optical and software development perspective that allow fluorescence based optical-imaging for tumor detection, as well as video-rate intraoperative image-guided surgery.<sup>12</sup> Reaching this level of complexity requires an improvement in fluorescent imaging modalities that face several challenges that include high tissue autofluorescence background levels and the complexity of deconvoluting chromophores with considerable spectral overlap. NIR excitation of PSs could be used for imaging, as it is less likely to induce autofluorescence, whilst narrow filters may also be employed to improve spectral separation. However, none of these solutions fully resolve the problem of PS spectral overlap with autofluorescence.<sup>79</sup> Hyperspectral imaging has thus been introduced in an effort to overcome this hurdle in PS imaging. The principle is based on the unmixing of several spectra following the acquisition of emitted light in each pixel to resolve and identify the fluorophores contributing to the resultant combined emission profile. The systems that have been developed allow the spectral deconvolution of chromophores that are separated by just a few

nanometers.<sup>80</sup> Mansfield *et al.* illustrated the basis of hyperspectral imaging by successfully unmixing the spectra emitted by five quantum dots, all characterized by a different emission profile. Each distinct quantum dot was conjugated to different markers that bind to different cellular components including the mitochondria, microtubules, proliferation marker Ki-67, nucleus, and actin. The five colors were successfully unmixed and a map representing the spatial distribution of each quantum dot marker, and thus each cellular component, was compiled.

Developing cutting edge-technologies such as hyperspectral imaging leads to the improvement of fluorescence imaging techniques that can be used for several purposes including fluorescence imaging for theranostics and image-guided resection. In fact, surgery remains the primary treatment for the majority of solid tumors, which requires complete resection to ensure a positive prognosis. Although the peripheries of some tumor types are well-defined and do not require the precautionary extraction of additional seemingly healthy tissue, other diffuse tumor types, including metastases, are more difficult to differentiate from normal tissues, or reside adjacently to crucial structures. Therefore, the accurate delineation of precise tumor margins is required to achieve more complete resections. Sensitive optical imaging techniques, such as fluorescence imaging can thus guide surgery. The clinically-approved extrinsic fluorophores indocyanine green (ICG) and fluorescein sodium are examples of fluorescence contrast agents that have been frequently used to assist intraoperative dissection.<sup>81</sup> More specifically, the endogenous PS protoporphyrin IX (PpIX) that accumulates in tumor tissue upon administration of the clinically-approved precursor, ALA, is currently in multiple clinical trials for assisting the resection of gliomas.<sup>82</sup> As shown in Figure 6, the white light images and PpIX fluorescence images acquired intraoperatively from a patient with glioma are contrasted to emphasize the powerful advantage of fluorescence imaging for increasing the accurate tumor detection and boundary delineation for surgical guidance.



**Figure 6. A)** Intraoperative white light image of the brain of a glioma patient with the respective fluorescence image following administration of ALA. The tumor is not visible to the naked eye, however, the endogenous PS PpIX preferentially accumulates in the tumor and enables its fluorescent detection and surgical guidance, which appears pink under blue light excitation in **B)** Figure reprinted from Widhalm *et al.*<sup>83</sup>

The field of fluorescence-guided surgery is less well-established, as compared to other imaging modalities. However, it has recently made outstanding strides in the clinical arena, mainly to precisely delineate tumor margins and for advancing real-time NIR PSs image processing techniques during surgical procedures, as comprehensively reviewed by Elliott *et al.*<sup>12</sup> During a Phase III clinical trial, image-guided tumor resection was performed following ALA administration on 322 patients with malignant glioma.<sup>84</sup> It was observed that the resection was complete for 65% of the patients operated on under fluorescence image-guided surgery, as compared to 36% for patients operated on with white light surgery.<sup>84</sup> Utilizing the inherent photosensitizing capacity of PSs used for fluorescence-guided resection, intraoperative PDT treatment can be used to eliminate the residual disease following surgery.<sup>32, 85</sup> In a single-center Phase III trial on 27 glioblastoma patients, fluorescence-

guided resection and post-operative PDT using a secondary administered PS doubled survival of patients, as compared to surgery performed under white light followed by radiotherapy (52.8 vs. 24.6 weeks, respectively).<sup>32</sup> Fluorescence-guided resection is also widely investigated for bladder cancer. It has been shown in several Phase III clinical trials that PS fluorescence-guided resection is significantly more complete than following white light cystoscopy. These different results were reviewed by Jochem *et al.*<sup>86</sup>

In addition to being used to guide resection, the fluorescence may also be used to diagnose or detect small nodules and metastases diffusely disseminated. For example, Zhong *et al* illustrated the ability to image the *in vivo* fluorescence signal of Visudyne® injected into the peritoneum of a mouse with disseminated micrometastases of human ovarian carcinoma (OvCa) using a high-resolution fiber optic microendoscopy modality.<sup>87</sup> They demonstrated that this method could be quantitative and that the signal intensity is proportional to the area of the nodules disseminated throughout the peritoneal cavities, thus enabling the longitudinal fluorescence-guided monitoring of treatment response.

Some PS molecules require strategies to enhance their selectivity by directing them to biomolecules or membrane-associated enzymes that are over-expressed on tumor cells or by manipulating cancer-activated metabolism pathways.<sup>12,81</sup> In 2011, van Dam *et al.* reported the first clinical utility of targeted tumor-specific intraoperative fluorescence imaging of OvCa to improve disease staging *in vivo* and to maximize the extent of radical cytoreductive surgery.<sup>88</sup> OvCa, 90-95% of which overexpress folate receptor- $\alpha$ , was targeted using a folate conjugate of fluorescein isothiocyanate, that could be expanded to the use of fluorescent PS conjugates. Selective theranostics using PSs have also been demonstrated preclinically using benzoporphyrin derivative (BPD) PS molecules conjugated to the anti-EGFR antibody, Cetuximab. The Cetuximab-BPD conjugates, termed photoimmunoconjugates (PICs), have been employed for the targeted imaging and PDT of non-resectable micrometastases of OvCa disseminated throughout the peritoneal cavity.<sup>11</sup> As presented in Figure 7 (A), the PICs also enabled longitudinal fluorescence microendoscopic imaging of the remaining disseminated OvCa tumor burden following cycles of tumor-targeted activatable photoimmunotherapy (taPIT). The modality also provided robust *in vivo* quantitation of the imaged tumor burden (Figure 7 (B)). The details and advancements of targeted PDT using PICs and the taPIT approach will be further described in the *Acquiring selectivity* section.

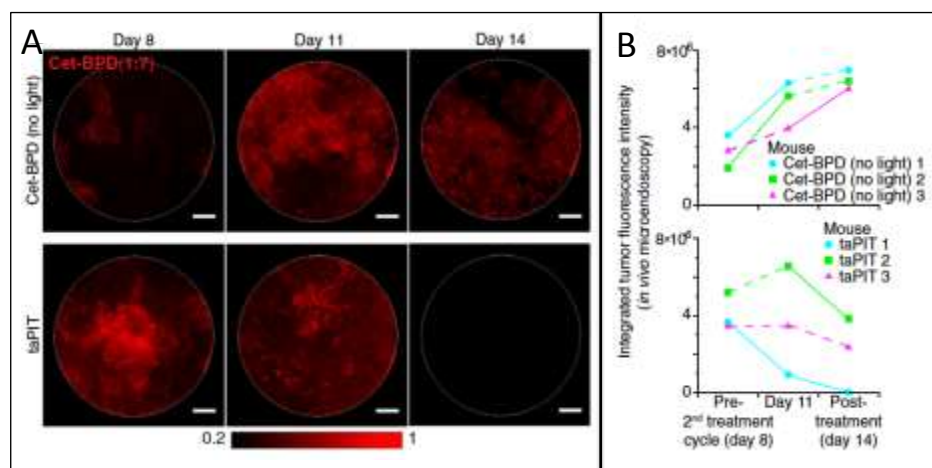


**Figure 7. A)** Images obtained by longitudinal *in vivo* fluorescence microendoscopy of tumor burden in a disseminated mouse model of OvCa treated with the Cet-BPD PIC without and with (taPIT) light activation (scale bar 100 $\mu$ m). **B)** Quantitative analyses of representative tumor fluorescence during the treatment. Solid lines indicate significant changes ( $P < 0.05$ , two-tailed unpaired t test). Figure adapted from Spring *et al.*<sup>11</sup>

Ultimately, advanced tumor-selective PNM formulations will be utilized in the same manner, where the fluorescence properties will provide the accurate delineation of tumor margins to aid surgical resection, and for the detection and photodynamic elimination of microscopic disease. Substantially prolonged circulation times of PNM formulations, as compared to free PSs or biological conjugates of PSs, will inevitably result in longer times

required to attain maximal tumor-to-normal ratios. Thus, careful investigations in PKs and tumor selectivity will be critical in identifying the optimal times required to utilize the full potential of the theranostic PNM formulations.

### Other imaging modalities

Theranostics also has a broader application and in this context, therapies such as chemotherapy, radiation therapy (RT), PDT or PTT can be combined with different clinical imaging techniques that include MRI, CT, positron emission tomography (PET) and NIR fluorescence.<sup>76</sup> As a platform for the combination of therapeutic agents with imaging agents, organic carriers such as liposomes, polymers or micelles<sup>90</sup> have been heavily investigated. In addition, inorganic nanoparticles, such as mesoporous silica nanocomposites, have also been utilized because of their biocompatibility and their high capacity for agent loading.<sup>91-93</sup> Two types of nanodots have also been explored in the context of theranostics: quantum dots<sup>94-96</sup> and carbon nanotubes,<sup>97</sup> both which are utilized as photoactive nanocarriers and as visible and NIR fluorescence imaging agents. Inorganic nanoconstructs such as iron oxide nanoparticles have also be functionalized with drugs to combined MRI with a therapeutic agent.<sup>98-100</sup> Significant interest has developed over the prospects of nanomaterials that intrinsically behave as both image contrast agents and as nanotherapeutics. One of the most prevalent examples is gold nanoparticles that, in addition to being physiologically inert, can be used as imaging agents that enhance the contrast of CT<sup>101</sup> and surface enhance Raman spectroscopy (SERS) imaging modalities.<sup>102</sup> Furthermore, gold nanostructures have also been shown to behave as efficacious therapeutics, such as radiosensitizers for RT,<sup>103, 104</sup> nanoparticulate carriers of PSs for PDT<sup>105, 106</sup> and as photothermal agents for PTT.<sup>17, 106</sup> Gadolinium-based nanoparticles have similarly drawn such attention for their ability to improve the efficacy of RT, whilst simultaneously enhancing MRI contrast, and thus allowing for the development of MRI-guided RT theranostic nanoconstructs.<sup>107</sup>

#### **a. Photoacoustic imaging to predict PDT efficiency**

In addition to being fluorescence contrast agents, PSs are also effective photoacoustic contrast agents. PAI, a 'light-in, sound-out' modality provides 3D optical absorption properties of the tissue being imaged at penetration depths that are significantly deeper than fluorescence imaging. Recent work by Mallidi *et al.*<sup>108</sup> and Ho *et al.*<sup>109</sup> showcases the ability of PAI to monitor PS tumor uptake and directs towards the ability to personalize dosimetry based on the PS concentration at the target site. As an alternative method to assess PDT efficacy without using PS photobleaching or <sup>1</sup>O<sub>2</sub> luminescence, PAI can also quantify changes in blood oxygen saturation levels induced during PDT by <sup>1</sup>O<sub>2</sub> generation. A recent preclinical study utilized PAI to highlight the critical role of tumoral oxygen saturation levels for monitoring responsiveness to PDT.<sup>111</sup> It was demonstrated that oxygen saturation evolution matched the tumor volume evolution and, as a consequence, was a reliable marker for PDT efficacy that could be studied non-invasively. For a PS-light-interval of 1 hour, oxygen saturation reduced to approximately 94% of the pre-PDT levels at 6 hours following treatment and increased by approximately 9% 18 hours later. In this same study, a threshold for oxygen saturation measured 6 hours and 24 hours post-PDT was established to predict tumor recurrence. Therefore, PAI could provide critical image guidance parameters when used in synchrony with PNM formulations to quantitatively monitor tumor uptake, assess the extent of the tumors response to PDT, and thus inform further cycles of therapy.

#### **b. Computed tomography to monitor PDT**

It has recently been demonstrated by preclinical and clinical studies that CT, a standard-of-care imaging method, may be used to predict the PDT dose required to treat patients with non-resectable pancreatic cancer.<sup>28</sup> CT remains the most widely used modality to diagnose and follow the evolution of pancreatic tumors. Aside from being a reliable method to predict PDT efficiency, this protocol has the unique advantage of potentially limiting the number of procedures that patients undergo. It is an X-ray based imaging technique based on the difference of X-ray absorption coefficients of body constituents, such as bone, tissues, and vasculature. CT contrast is usually enhanced using iodine solutions, a high Z-number element that locally increase X-ray absorption.<sup>112</sup> Elliott *et al.* published a preclinical study performed on rabbit orthotopic pancreatic cancer that compares several tumor controls such as blood volume, blood flow and vascular permeability surface area obtained from CT images.<sup>113</sup>

They emphasized that blood volume may be a determinant of treatment response because the lower it is, the lower the PS dose delivered. This pre-clinical study highlighted the potential of CT imaging to map the PDT dose, driven by the light attenuation in tissues. Jermyn *et al.* recently proposed a clinical study performed on 15 patients with locally-advanced adenocarcinoma that aimed to prove the potential of using CT imaging to predict PDT efficiency and thus adapt the treatment protocol.<sup>28</sup> In this trial, pre-treatment and post-treatment contrast-enhanced CT scans were used. Venous blood volumes were calculated for each patient using the pre-clinical CT and then compared to the necrotic volume induced by the PDT measured using the post-treatment CT scan. The CT-derived venous blood content highly correlated with the necrotic volume normalized to the PS dose. The findings indicated that a pre-treatment CT scan may allow the prediction of the necrotic volume after PDT and, as a consequence, may inform the total PDT dose required, individualized to each patient. This clinical study corroborates the previous assumption that blood volume is a limiting factor to the effective PDT dose administered. The utility of this standard-of-care procedure could be expanded to predict patient response to PDT using parenteral PNM formulations and subsequently guide the personalization of the treatment.

### c. Cerenkov emission imaging to monitor RT and PDT

Cerenkov luminescence imaging is a less common, state-of-the-art bioimaging technique currently being developed to monitor treatments such as RT, and can potentiate and guide PDT using forward-looking PNM formulations. Cerenkov imaging has recently gained substantial clinical interest with particularly strong implications in quantifying the effective dose of ionizing radiation deposited during RT.<sup>114, 115</sup> Cerenkov optical emission spanning the UV-Visible spectrum is generated by charged particles in a dielectric medium travelling faster than the phase velocity of light in the same medium and can activate nearby PSs localized at the site of RT treatment.<sup>115, 116</sup> Recently, the proof-of-concept of video rate Cerenkov imaging was presented, providing real time insight to the effective three-dimensional radiation dose deposited during RT, as illustrated in Figure 8.<sup>117</sup> Although the proof-of-concept was proposed for RT of breast cancer, this dosimetry protocol may be expanded to combination treatment regimens that combine RT with PDT, providing more precise, complete and tolerable irradiation procedures. Axelsson *et al.* showed that Cerenkov emission is sufficient to activate the fluorescence of a PS, PpIX, although studies investigating the PDT efficacy of PSs activated using Cerenkov emission from external radiation are pending.

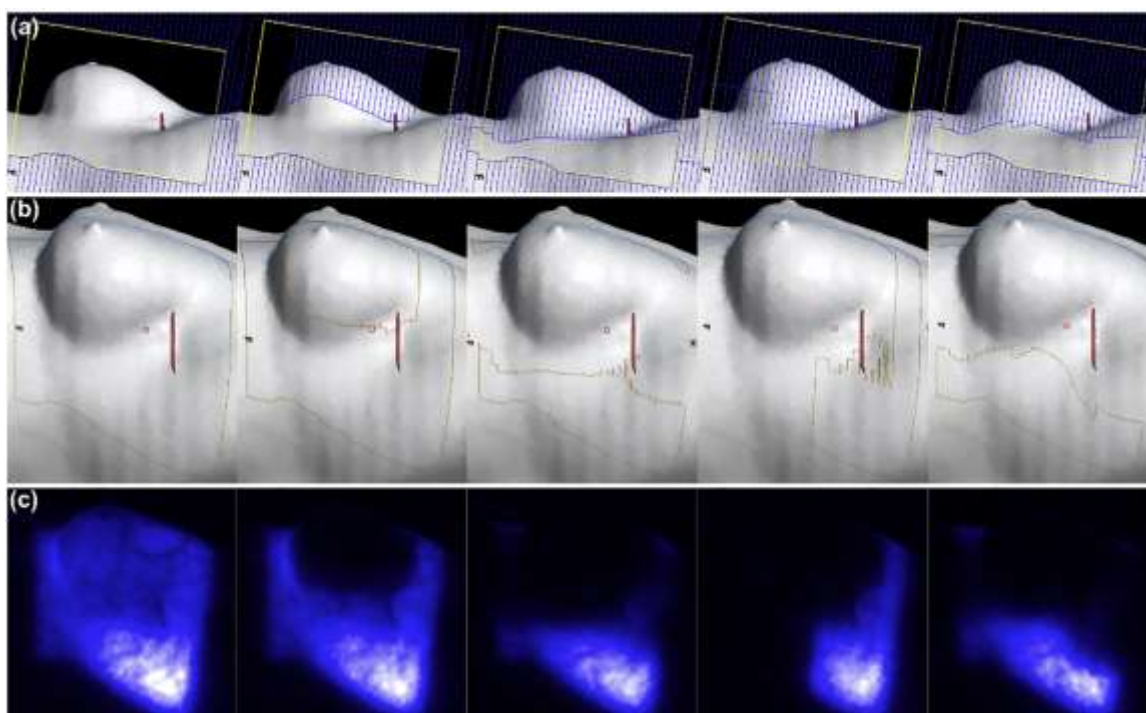


**Figure 8.** A) The beam's-eye-views of the applied RT fields. The blue lines refer to the multi-leaf collimator that blocks the

radiation from these areas. **B)** The surface projection on the skin from the posterior oblique portion to be irradiated. **C)** Cerenkov luminescence images during RT of the posterior oblique field. The areas with the highest intensity correspond to the tissue receiving the highest effective radiation dose. Reprinted from International Journal of Radiation Oncology, 89(3), Jarvis *et al.*<sup>117</sup> *Cerenkov video imaging allows for the first visualization of radiation therapy in real time*, 615-622. Copyright (2015), with permission from Elsevier.

$\beta$ -emitting radionuclides used for PET imaging have also been known to exhibit high yields of Cerenkov emission, without the need for external activation using ionizing radiation.<sup>118</sup> Katogiri *et al.* recently proposed the use of Cerenkov radiation from a  $\beta$ -emitting radionuclide to activate type I photochemical reactions for PDT.<sup>119</sup> In this study, the authors reported the use of  $^{64}\text{Cu}$ , a radionuclide clinically used for PET imaging, to excite photocatalytic titanium dioxide ( $\text{TiO}_2$ ) nanoparticles through its simultaneous emission of Cerenkov radiation. This pre-clinical study demonstrated the potency of the PDT combination treatment in that tumor volumes were reduced below the detectable range when  $\text{TiO}_2$  NPs were used in combination with  $^{64}\text{Cu}$ . However, tumor volumes remained approximately 400 mm<sup>3</sup> when  $\text{TiO}_2$  nanoparticles were used in conjunction with non-radioactive Cu, approximately 550 mm<sup>3</sup> when  $^{64}\text{Cu}$  was used alone, and remained above 650 mm<sup>3</sup> in the no treatment controls. Co-encapsulation of a  $\beta$ -emitting radionuclide with a PS in a combined novel PNM construct may promote spatiotemporally-controlled, Cerenkov-induced photodynamic activation of the PDT agent held its immediate vicinity. Furthermore, PET imaging using  $\beta$ -emitting radionuclides typically contrasts tumors by providing functional information, such as glucose metabolism and oxygen consumption, both critical parameters that can simultaneously monitor the extent of PDT treatment response in real time.

Although in the early stages of discovery, deep tissue PDT activation using localized Cerenkov emission provides clinically valuable advantages of either exogenous induction by ionizing radiation during RT or endogenous activation using PET probes, which can be used in concert with common clinically-accepted imaging modalities. Although PDT activation using Cerenkov radiation from  $\beta$ -emitting radionuclides simplifies the clinical procedure required with externally activation RT and the critical irradiation parameters associated with it, the spatial selectivity for PDT activation is entirely lost. Cerenkov-mediated PDT using an integrated PNM formulation containing a  $\beta$ -emitting radionuclide and a PS becomes a systemically active treatment modality, where the PK of the nanoconstruct governs induction of toxicity. Toxicity of the liver, spleen and other organs where nanoparticles tend to accumulate is likely to be observed, and therefore, tailoring size and surface properties of the PNM formulation becomes even more critical.

Additional modalities utilizing the unique inherent photoactivity of novel nanoconstructs to overcome the limited penetration of light through tissue rely on their direct interaction with deeply penetrating ionizing radiation or NIR light. Photoactive inorganic nanocrystals, such as upconverting nanoparticles<sup>71</sup> or nanoscintillators,<sup>70, 121</sup> respectively, are emerging as advanced deep-tissue PNM formulations, when combined with PSs to locally produce RMS at anatomical sites typically inaccessible to external photoirradiation. Because of the clinical implications of X-rays of NIR light,<sup>122</sup> currently used for imaging and RT, these nanocrystals exhibit theranostic properties when combined with therapeutic PSs. When excited with ionizing radiation, scintillation nanoparticles emit light spanning the UV/visible/NIR spectrum and can thus internally activate associated PS with wavelengths of light typically inaccessible at such tissue depths.<sup>70</sup> Similarly, upconverting nanoparticles absorb NIR light that penetrates tissue deeper than visible wavelengths and locally upconvert it to shorter wavelengths that efficiently excite associated PS molecules.<sup>71</sup> Moreover, inorganic metal nanoparticles, such as gold nanoparticles, may elicit an inherent therapeutic effect including PTT or radiosensitization during RT, and their contrast-enhancing imaging properties can potentiate image guidance using CT. The diverse selection of nanomaterials provides a highly attractive pool of potential theranostic platforms; however, each nanomaterial can carry its own health risks and its clinical progression depends on the stringent investigations required to rule out immediate hazards or adverse health effects due to prolonged exposure. These concerns are more prominent when investigating inorganic nanomaterials composed of heavy metal atoms (noble metal nanoparticles), iron compounds (magnetic fluids), rare-earth metal compounds (up-converting and scintillating nanoparticles), inorganic oxides (silica, titania and

zinc oxide nanoparticles) and transition metal composites (quantum dots). This concern is directly evident by the fact that currently, Feraheme<sup>®</sup>, a polyglucose sorbitol carboxymethylether-coated iron oxide nanoparticle formulation, is the only remaining approved inorganic nanotherapeutic following the withdrawal of four previously-approved nanoformulations.<sup>123</sup> Although the reasons for their withdrawal were ambiguous, a warning emphasizing potential adverse immune reactions to Feraheme<sup>®</sup> was released by the FDA in 2015. As a consequence of the delay in the clinical translation of inorganic nanomaterials, this review will mainly focus on the advancement of nanoscale therapeutics and diagnostics composed of organic, biodegradable materials that are currently in clinical use.

## Photochemistry and nanomedicine: meeting unmet clinical needs

### Barriers to drug delivery

#### a. Tailoring nanomedicines to tumor physiology

Nanomedicine has been primarily introduced to reduce the inherent toxicity of cancer therapeutics by improving their selectivity towards tumor tissue. It is important to emphasize that as a cancer therapy, PDT is largely non-toxic in the absence of light. However, many PSs for PDT are hydrophobic, rendering their systemic administration impossible without the use of organic solvent mixtures. An example of such PSs is Foscan<sup>®</sup>, an EMA approved PDT agent (mTHPC/temoporfin) for the treatment of head and neck cancers, which is administered systemically in ethanol:propylene glycol (40:60 v/v). To reduce the need for such solvents and their associated toxicities, the application of nanoparticle encapsulation was primarily employed for PDT to render PSs compatible with physiological media, such as blood plasma. Efforts towards the nanoparticle encapsulation of photosensitizing agents have led to the development of a multitude of 'second generation' PSs, of which Visudyne<sup>®</sup> and Foslip<sup>®</sup>, a liposomal derivative of Foscan<sup>®</sup>, are notable examples.

An important unanticipated feature of nanoparticle encapsulation of PSs for their improved water solubility is the significantly increased selectivity for tumor tissue. For instance, Reddi *et al.* were among the first to explore liposomally encapsulate zinc phthalocyanine (ZnPC) and its drug delivery *in vivo*. Following the injection of 0.5 mg/kg<sup>-1</sup> ZnPC in 1,2-dipalmitoyl-*sn*-glycero-3-phosphocholine (DPPC) liposomes, tumor tissue accumulated relatively high levels of ZnPC (0.6 µg/g), compared to <0.1 µg/g in the muscle tissue surrounding the tumor 24 h following intravenous administration.<sup>124</sup> Given that PNM formulations can also improve the PS selectivity for tumor tissue, a variety of different types of nanocarriers have been investigated for the encapsulation of hydrophobic and hydrophilic PSs. Among the most studied are liposomes, (polymeric) micelles, and polymeric solid-lipid nanoparticles.<sup>125, 126</sup> Many other investigators have reported that these PNM formulations also improve the tumor-to-normal ratio of PS *in vivo*, as summarized in Table 1.<sup>127-129</sup>

**Table 1.** Drug selectivity for the target site, displayed as tumor:normal tissue ratio as a function of respective PNM formulation, type of PS, and time interval (hours post-injection). Single asterisks (\*) indicate tumor:muscle ratio, double asterisks (\*\*) indicate tumor:skin ratios. Hashtags refer to specific types of pancreatic tumor xenografts, where a single hashtag (#) refers to AsPC-1 pancreatic tumors and double hashtags (##) refer to PANC-1 pancreatic tumors. The PSs formulated in the studies summarized within the table are zinc phthalocyanine (ZnPC), meta-tetra (hydroxyphenyl)chlorin (mTHPC), Hypocrellin A and benzoporphyrin derivative (BPD). Ingredients of the PNM formulations include 1,2-dipalmitoyl-*sn*-glycero-3-phosphocholine (DPPC), 1,2-dipalmitoyl-*sn*-glycero-3-phospho-(1'-*rac*-glycerol) (DPPG), 1,2-distearoyl-*sn*-glycero-3-phosphoethanolamine-*N*-(polyethylene glycol) (DSPE-PEG), dimethylsulfoxide (DMSO) and egg phosphatidylcholine (EPC).

PNM formulation	Photosensitizer	Tumor:normal ratio	Time post-injection	Reference
DPPC	ZnPC	7.5*	24 h	Reddi <i>et al.</i> (1987) <sup>130</sup>
DPPC:DPPG (9:1)	mTHPC	1.5, 3.8, 9 * 1.5, 1, 1 **	3 h, 6 h, 24 h	Reshetov <i>et al.</i> (2013) <sup>131</sup>
DPPC:DPPG:DSPE-PEG	mTHPC	6, 10, 10 *	3 h, 6 h, 24 h	

(9:1:1)		1.5, 2.2, 2 **		
DPPC:DPPG:DSPE-PEG (9:1:1)	mTHPC	10.8 **	7.3 h	Bucholz <i>et al.</i> (2005) <sup>132</sup>
(DMSO)	Hypocrellin A	1.9, 2.6, 1.5 * 1.2, 1.2, 1.5 **	3 h, 6 h, 24 h	Wang <i>et al.</i> (1999) <sup>133</sup>
EPC	Hypocrellin A	3.3, 3, 2.5 * 2.1, 2.1, 1.1 **	3 h, 6 h, 24 h	
Visudyne®	BPD	1.7, 5 #*	3 h, 24 h	O'Hara <i>et al.</i> (2009) <sup>134</sup>
		1.4, 3.5 ##*		
		1.2, 1.1 ###* 1.9, 3 ###**	3 h, 24 h	

The increased propensity of nanoparticles to accumulate at the tumor site is primarily effectuated by the EPR effect. The EPR effect is the result of the high metabolic demand of the proliferating tumor mass and the resultant aberrant fenestrated angiogenic vasculature that rapidly form, in addition to poor lymphatic drainage of the tumor interstitial fluid.<sup>135</sup> The EPR effect allows for the extravasation of high-molecular weight plasma components, and can be exploited by nanocarriers of anti-cancer drugs.<sup>136</sup> In order for nanocarriers to fully utilize the EPR effect, a steric barrier that reduces non-specific nanoparticle-protein interactions is crucial to achieve prolonged systemic circulation times. Steric stabilization of nanocarriers with hydrophilic barrier molecules, such as PEG that grants stealth-like properties to nanocarriers can significantly reduce absorption by the liver, kidney, spleen, and the reticuloendothelial system (RES).<sup>137</sup> Thus, PEGylation enhances the extent to which the nanoparticles extravasate at the tumor site. For PDT specifically, BPD-containing liposomes that were sterically stabilized with palmityl-D-glucuronide exhibited prolonged circulation times and increased the therapeutic efficacy of the PS, in comparison to treatment with either free BPD or non-sterically stabilized liposomal BPD.<sup>129</sup> PNM formulations utilized for non-photochemical PTT applications have also been formulated in a similar manner using identical steric stabilization approaches. An interesting advancement in the field of thermal PNM formulations is the development of the porphysome, a self-assembled nanovesicle consisting of porphyrin-conjugated phospholipid bilayers that was pioneered by Lovell *et al.* and was PEGylated to improve steric stability.<sup>138</sup> Due to the high proximity of the individual lipidated porphyrin molecules within the porphysome bilayer, the chromophores exhibited up to 1500-fold fluorescence quenching and were capable of inducing phototheramlization at levels comparable to gold nanorods. The photoacoustic effect that is concurrent with photothermalization was also leveraged for imaging using PAI. Furthermore, the unique structures were expanded to pyropheophorbide, zinc pyropheophorbide and bacteriochlorophyll porphysome variants. Doxorubicin was also encapsulated within the porphysome to yield a photothermal iteration of Doxil®.

Aside from steric stability and stealth-like properties, appropriate sizing of nanocarriers is essential for the efficacy of a nanosized drug delivery platform. Sterically stabilized liposomes smaller than 70 nm were shown to be retained by the liver,<sup>139</sup> whereas liposomes larger than 220 nm were effectively taken up by the spleen.<sup>140</sup> As such, it was demonstrated that PEGylated liposomes with sizes between 160-220 nm exhibited the longest circulation times *in vivo*.<sup>140</sup> With respect to exploiting the EPR effect for tumor-specific delivery, the vascular fenestrations of tumor-associated vessels are approximately 100-600 nm in diameter.<sup>141</sup> In comparison, healthy vasculature typically displays fenestrations smaller than 10 nm in diameter.<sup>142</sup> Thus, tuning the nanocarrier size within the range of 160-220 nm in diameter will result in optimal circulation times and maximal global tumor drug delivery. These physiological characteristics of tumor vasculature can inform the design on nanocarriers, although many factors will influence the success of nanotherapeutics, which include tumor penetration and cellular internalization. These factors include nanoparticle size, formulation material, PEG density, geometry and electrostatics, all of which must be independently tuned in concert for a given newly-developed PNM formulation.

#### **b. Tailoring tumor physiology to nanomedicines using photochemistry**

Given that the abnormal and leaky tumor vasculature contributes to tumor growth and disease progression, there are currently ongoing investigations geared towards the normalization of the vasculature with the aim of inhibiting

disease progression.<sup>143</sup> For instance, a recent study by Chauhan *et al.* reports on the normalization of the abnormal tumor vessels by blocking vascular endothelial growth factor receptor-2 (VEGFR-2) signaling in angiogenic vascular endothelial cells.<sup>144</sup> With respect to nanomedicine, it was shown that vessel normalization reduced the size of the vascular fenestrations and hindered the delivery of 125 nm quantum dots, whilst improving tumor penetration of 12 nm quantum dots.<sup>144</sup> Vascular normalization is an example of how modulating the tumor physiology can enhance the homogenous intratumoral distribution and, subsequently, the therapeutic index of small molecular weight drugs and nanoparticles.<sup>145</sup>

Conversely, the expansion of tumor vascular fenestrae and vascular permeabilization has been achieved by the controlled photochemical activation of a PS when confined to the intravascular space; a phenomenon reported early on by Henderson *et al.*<sup>146</sup> and many others.<sup>6, 147-150</sup> At sufficiently low PDT doses, vascular PDT (vPDT) has been shown to further enhance the EPR effect and to improve the extravasation of nanomedicines into the tumor. Low-dose vPDT using the PS BPD was specifically shown to enhance the EPR effect in an orthotropic rat prostate cancer model.<sup>147</sup> The tumor uptake of 2,000-kDa FITC labeled dextran particles was enhanced following BPD-induced vPDT with a short 15 min PS-light interval.

More recently, ferritin protein nanocages loaded with the ZnF<sub>16</sub>Pc PS and surface functionalized with RGD peptide were developed by Zhen *et al.* (Figure 9).<sup>151</sup> These actively targeted nanoparticles, referred to as P-RFRT, selectively bound to  $\alpha_v\beta_3$  integrin receptors on endothelial cells in the tumor vasculature. The irradiance was optimized to 14 mW/cm<sup>2</sup> (50-300 mW/cm<sup>2</sup> is used for conventional PDT) for the maximal EPR enhancement, with minimal collateral toxicity to the tumor vasculature. Following P-RFRT-mediated vPDT, enhanced tumor accumulation of varying sized cargoes, such as albumin, quantum dots and iron oxide nanoparticles, was demonstrated in multiple xenograft tumor models. Efficacy studies were carried out under the same vPDT conditions followed by administration of Doxil<sup>®</sup> in a 4T1 tumor model. Importantly, controls studies ~~with~~ in animals treated with P-RFRT-mediated vPDT alone showed tumor growth rates similar to saline treated animals, confirming the absence of PDT-related tumor damage. In contrast, animals treated with P-RFRT-mediated vPDT followed by Doxil<sup>®</sup> treatment experienced a potent tumor-growth inhibition of 85.9%, a 75.3% improvement in efficacy over treatment with Doxil<sup>®</sup> alone.

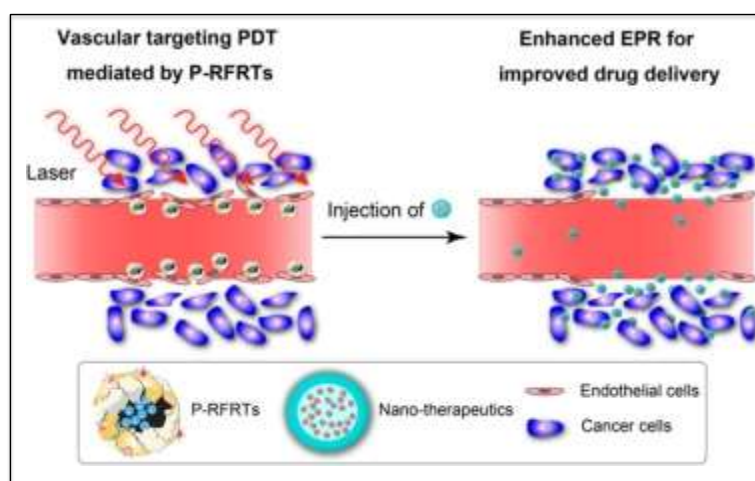


**Figure 9.** vPDT assisted EPR effect for higher tumor extravasation of nanoparticles. Proposed mechanism of action of ferritin nanoparticles loaded with ZnF<sub>16</sub>Pc PS and actively targeted with RGD-peptide (P-RFRT).<sup>151</sup> P-RFRT mediated vPDT action first increases gaps in the tumor vasculature, thereby facilitating deeper penetration of subsequently administered therapeutic nanoparticles. Figure adapted with permission from Zhen *et al.*<sup>151</sup> copyright 2014 American Chemical Society.

The tumor vasculature varies considerably between different cancer types and can influence the outcome of vPDT.<sup>150</sup> Araki *et al.* employed a porphyrin-based PS loaded within PEG-poly(lactic acid) nanoparticle (PN-Por), to

increase vascular permeabilization, which was subsequently followed by chemotherapy using liposomal paclitaxel (PL-PTX).<sup>152</sup> The study was performed in murine models of a colon-26 adenocarcinoma (C26) and a B16BL6 melanoma, which vary considerably in their vascular composition and permeability. In the C26 tumor model, PN-Por-mediated vPDT itself caused considerable tumor damage *via* endothelial cell apoptosis; however, the subsequent PL-PTX regimen did not improve outcome. Conversely, in the B16BL6 model, vPDT enhanced diffusion of PL-PTX into the tumor core and enhanced the efficacy of PL-PTX treatment. The reason for this differential vascular response between the two tumor models was associated with pericyte coverage and vessel diameter. Thus, the overall applicability of vPDT to enhance EPR based nanoparticle accumulation depends on the precise control over light dosage, a better understanding of the different innate microvasculature of tumors and on the continued development of tailored vasculature targeted nanoparticles.

An additional physical barrier in the tumor microenvironment is the stroma. The role of the tumor stroma in cancers, such as pancreatic cancer, has become increasingly regarded as a significant hindrance to drug delivery.<sup>153</sup> It has been found that a dense avascular tumor stroma prohibits drug diffusion throughout the tumor tissue.<sup>154</sup> In this respect, photochemical approaches may be utilized to improve the delivery and diffusion of cancer therapeutics by disrupting the rigid stromal barriers. With the use of 3D culture models, it is known that pancreatic and ovarian tumor spheroids that develop in an extracellular matrix become increasingly insensitive to chemotherapeutic agents.<sup>155</sup> However, neoadjuvant PDT was shown to resensitize the spheroids to chemotherapy by disrupting the nodule's three-dimensional architecture.<sup>155, 156</sup> As such, integrating photochemistry into nanomedicines may ultimately enable the use of forward-looking PNM formulations that can enhance their own delivery into tumors using the assistance of vPDT and even throughout the stroma.

### Limiting Toxicity

Even though PDT is largely non-toxic in the absence of light, there are some toxicological issues associated with the therapy. PSs that are systemically administered in free form typically accumulate at high concentrations in the liver, spleen, lungs, and kidneys.<sup>157-159</sup> The effective absorption of the PS by these organs potentially reduces the overall amount of PS that can accumulate at the tumor site, ultimately requiring higher drug concentrations to achieve the desired effect. Although the near lack of toxicity in the absence of light constitutes a major benefit of PSs in relation to other cancer therapeutics, PS accumulation in the skin has been a prominent adverse event associated with early PDT agents that lead to skin toxicity and ethical considerations regarding the quality of life of terminally ill patients.<sup>160</sup> However, the later 'second generation' PSs have minimized these initial problems with skin phototoxicity. In contrast to conventional drugs, where the need for formulation has been driven by non-specific toxicity, the motivation of formulating PS is often a lack of solubility. Nanoformulations that enhance the solubility and molecular monomerization of PS in physiological environments can thus maximize their photoactivity *in vivo*.

With respect to PDT, several liposomal formulations containing the PS mTHPC, also known as temoporfin or Foscan®, have been developed by Biolitec Research GmbH™. These include a conventional liposomal formulation (Foslip®) and a PEGylated liposomal formulation (Fospeg®). The PDT efficacy of both formulations was superior to that of the free PS.<sup>161, 162</sup> With respect to tumor selectivity, Fospeg® had significantly faster tumor accumulation kinetics and a higher tumor selectivity in comparison to Foslip®.<sup>163, 164</sup> These results illustrate the significance of steric stabilization with respect to the efficiency of drug delivery and to the potential for reducing off-target phototoxicity with PS nanocarriers.

Reducing the toxicity has been employed extensively for cancer therapeutics so as to reduce the morbidity of these treatments. A fundamental paradigm for reducing toxicity using nanoparticle encapsulated drugs is Doxil®. This formulation contains high intraliposomal doses of doxorubicin, and was primarily developed to address the need for reducing the drug's cardiac toxicity. Liposomes with high concentrations of doxorubicin, and their EPR-mediated accumulation in tumor tissue following systemic injection led to the slow release of doxorubicin at the

tumor site. This nanomedicine showed an improvement in drug delivery and therapeutic efficacy, while significantly reducing the adverse toxicity.<sup>3</sup>

Photochemistry can play a unique role in providing an additional method for reducing toxicity of diagnostic and therapeutic agents by facilitating the controlled drug release from nanocarriers specifically at the site of the tumor. By using a PNM formulation co-encapsulating both photosensitizing and therapeutic agents, which preferentially accumulates at the tumor site, subsequent irradiation of the lesions results in the oxidative release of the adjuvant therapeutics from the nanocarrier. While the PNM formulation encapsulation shields the drug from systemically exerting its effects, the spatiotemporal controlled phototriggered release upon irradiation confines the toxicity of the drug to the irradiated site. This technique has been successfully applied by Spring *et al.*, who showed that XL184 (cabozantinib, Cometriq®, a c-MET and VEGFR-2 inhibitor) entrapped in a polymeric nanoparticle, further encapsulated in photoactive lipid layers, was effective at a dose that was 1000-fold lower than the total dose of free XL184 administered.<sup>51, 165</sup>

### Limitations in cellular uptake

Once agents reach the target tumor tissue, another barrier to achieving their anti-neoplastic effect is the hurdles they encounter upon attempting to enter the cell. Cancer cells have evolved multiple mechanisms to evade chemical insult, the first of which are transmembrane efflux transporters, such as P-glycoprotein and ATP-binding cassette transporters (ABCs). In this context, some nanoparticles have drawn particular interest as they can evade transporter efflux of their therapeutic payload by delivering the drugs intracellularly through alternative endocytic pathways. Xu *et al.* presented a comprehensive and focused review on the mechanisms through which drug-encapsulating nanoparticles, termed nanotransporters when used for this specific role, evade common drug efflux transporters that give rise to multi-drug resistance in a variety of cancers.<sup>166</sup> However, although nanoparticles can increase intracellular delivery of cytotoxic and cytostatic agents, endosomal escape of these agents into the cytosol to perform their function can oftentimes be a second barrier that has been addressed by a photochemistry-based intervention termed photochemical internalization (PCI). Pioneered by the team of Dr. Kristian Berg in 1995, PCI utilizes low PS and light doses that are only sufficient for the selective disturbance of endosomal membranes, resulting in cytosolic release of the endosomal therapeutic contents.<sup>167, 168</sup> PCI using the PS aluminium phthalocyanine disulfonate and bleomycin as the therapeutic agent, has been reported to improve the destruction of the peripheral margins of a human TAX-1 xenograft model, as compared to PDT when applied before external beam radiotherapy.<sup>169</sup> The technique has rapidly progressed into the clinic and the first clinical trial using the PS tetraphenylchlorin disulfonate (Amphinex®) and bleomycin as the active chemotherapeutic for cutaneous cancers was completed in 2009.<sup>170</sup> Currently, a Phase I/II trial using the PS Amphinex® and gemcitabine as the chemotherapeutic for the treatment of inoperable cholangiocarcinoma is ongoing.<sup>171</sup> Recently, an elegant study reported the efficacy of haematoporphyrin-mediated PCI for the cytosolic delivery of camptothecin encapsulated within PEG-polyacetal block copolymer nanoparticles that were labile to both acid hydrolysis and photolysis. Photoirradiation mediated the release of camptothecin from the nanoparticle as well as the endosomal compartment, and enhanced the phototoxicity of HeLa cells by up to 40%, as compared to the irradiation of cells incubated with a combination of free PS and camptothecin.<sup>172</sup> Understandably, PCI requires a delicate balance in the PS and light dosimetry parameters, which if they exceed a certain PS and light threshold, induce PDT tissue damage. Furthermore, it is probable that varying degrees of PDT and PCI can simultaneously occur during the irradiation of the same tumor as a result of the complex light scattering profiles throughout tissue. Thus, a definitive distinction between the two photochemical modalities can often be challenging *in vivo*.

### Acquiring Selectivity

The concept of tumor-targeted therapeutics has been pursued since Paul Ehrlich's proposal of the 'magic bullet', which comprises of a targeting moiety conjugated to a cytotoxic agent.<sup>173, 174</sup> Antibody conjugates therefore represent an early version of nanomedicine agents. This vision is realized with antibody-based platforms such as

immuno-toxins<sup>175, 176</sup> and antibody-drug conjugates (ADCs).<sup>177-181</sup> Lately, the field of ADCs has rapidly expanded following the FDA approval of Brentuximab vedotin and Trastuzumab emtansine, as well as the continued clinical development of several candidates.<sup>182</sup> Parallel to ADCs, PSs have been conjugated to antibodies to form PICs.<sup>183, 184</sup> Following seminal work by Levy *et al.*<sup>185-187</sup> many examples of PICs have been reported by us<sup>11, 188-198, 199, 200</sup> and others,<sup>184, 201-205</sup> where biological conjugates of PSs have been deployed as tumor-targeted agents for photoimmunotherapy (PIT) over the past three decades. While conceptually similar to ADCs, PICs present several additional advantages. In addition to antibody targeting, PICs afford a second level of selectivity by focused delivery of light to activate PDT mediated cytotoxicity only in the tumor microenvironment. Unlike ADCs, the inherent fluorescence property of the PS allows optical imaging, thus enabling various diagnostic modalities as discussed in the *Theranostics* section.<sup>11, 201, 206</sup> ADCs and immuno-toxins, antibody conjugates of toxins, require cellular internalization followed by cytosolic release of the cytotoxic cargo, often requiring elaborate endosomal escape strategies. In contrast, PIT does not necessarily require internalization of the PIC and can kill cells even whilst being localized to the cell surface.<sup>89, 207</sup> PICs are able to realize mechanistically distinct features of PDT such as its ability to sensitize chemo-resistant cancer cells<sup>156, 208</sup> and elicit the bystander effect to extend toxicity to neighboring supporting cells beyond the primary cancer cell target.<sup>209-211</sup> Despite these promising features and tremendous efforts there are currently no FDA approved PICs.

Goff *et al.* employed primary cells obtained directly from patient tissues, spanning multiple cancer types and stages of resistance, to develop various PICs.<sup>196</sup> The authors reported the use of a murine antibody, OC-125, which recognizes the cell surface antigen CA 125 expressed by 80% of non-mucinous human OvCa. The PS chlorin e6-monoethylenediamine monoamide (CMA), linked to a poly-glutamic acid polymer, was site-specifically conjugated to oxidized carbohydrate residues of OC-125 to form an anionic PIC. This anionic PIC was also tested *ex vivo* in ascites or pleural fluid cells from 15 patients with ovarian and non-ovarian cancers. Viability studies in these mixed-cellular models exerted a selective PDT efficacy in OvCa cells over non-ovarian cancers. The killing of non-cancer cells was attributed in part to the bystander effect of PDT. Importantly, OvCa cells from end-stage drug-resistant patients also showed a significant response to the PDT. These chemoresistant cells often lack cross-resistance to PDT. In fact, sublethal doses of PDT can be used to resensitize drug resistant cancer cells to chemotherapy. These encouraging results prompted explorations on the combination of PICs with traditional chemotherapy agents, which otherwise would be sub-optimal in drug-resistant cancer cells. Such mechanistically non-overlapping combinations of PDT with chemotherapy could overcome chemoresistance and potentially exert a synergistic effect in stubbornly refractive tumors.<sup>156, 193, 212</sup> Duska *et al.* used the F(ab')<sub>2</sub> fragment of OC-125 conjugated to a cationic poly-lysine polymer that was modified with multiple chlorin e6 (Ce6) PS molecules.<sup>194, 208</sup> This PIC was assessed in 5 human cancer cell lines as well as 19 primary cultures obtained from solid tumors and ascites samples derived from platinum-responsive and platinum-resistant OvCa patients. *Ex vivo* viability studies using a combination of PICs with cisplatin demonstrated a potent 12.9-fold higher synergistic effect against platinum-resistant cells.<sup>208</sup>

PICs have also been designed to target the tumor neovasculature to improve the selectivity of vascular PDT (vPDT), which is discussed in greater detail in the *Manipulation at the macrophysiological level* section. Palumbo *et al.* employed a PIC called SIP(L19)-PS, which was composed of a porphyrin PS conjugated to an anti-L19 antibody. The PIC targeted the spliced extra-domain B of fibronectin in the small immune protein format, a marker of tumor angiogenesis (Figure 10 (A)).<sup>89, 207</sup>

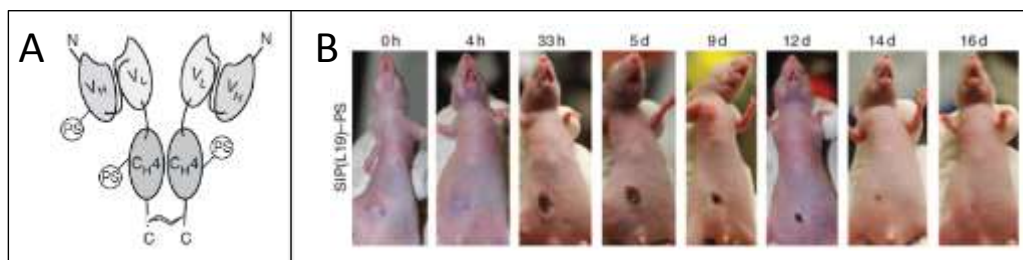


**Figure 10.** **A)** Schematic representation of tumor vasculature targeted PIC composed of an antibody, in the small immune protein format (SIP), and PS molecules coupled to the antibody's lysine residues.<sup>89</sup> **B)** Demonstration of SIP(L19)-PS efficacy in a subcutaneous xenograft model of squamous-cell carcinoma at different time points following targeted PDT.<sup>89</sup> Reprinted by permission of Macmillan Publishers Ltd. on behalf of Cancer Research UK: Paulmbo *et al.*<sup>89</sup> British Journal of Cancer, copyright 2011.

This PIC selectively localized to tumor vessels *in vivo* and, upon irradiation, led to the complete eradication of a subcutaneous squamous cell carcinoma tumor at relatively low administered PS dosages. Figure 10 (B) shows the regression of the subcutaneous tumor up to 16 days following PDT. Interestingly, no tumor relapse was observed for up to 100 days after treatment. The authors confirmed the role of natural killer cells in the observed long-term response, as inhibition of the natural killer cells resulted in the poor retardation of tumor growth following PDT, eventually leading to disease progression. Finally the authors demonstrated the selective staining of vascular structures by the L19 antibody, amongst other vascular targeting antibodies, in normal skin and squamous cell carcinoma lesions extracted from patients. Occult, non-resectable drug-resistant micrometastases spread throughout the peritoneal cavity are widely responsible for treatment failure and disease relapse in OvCa.<sup>11,88</sup> To tackle this challenge, Spring *et al.* enabled a further level of selectivity in the PIC platform, namely tumor cell activation.<sup>11</sup> Specifically this next generation PIC (Cet-BPD) was composed of the EGFR-specific chimeric antibody Cetuximab and the FDA-approved PS BPD (Figure 11).

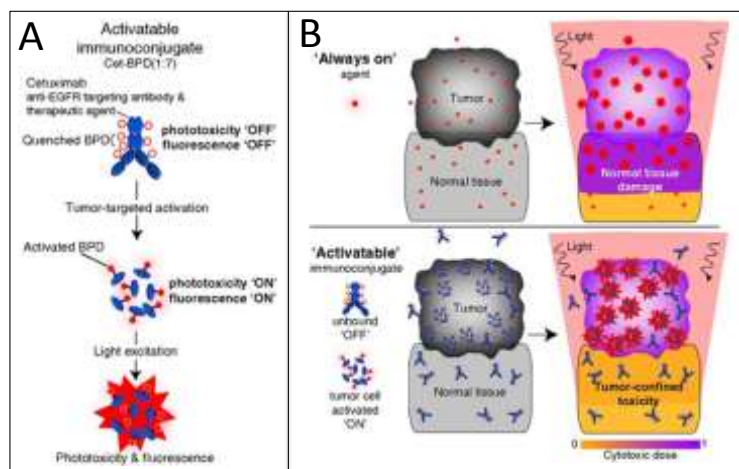


**Figure 11.** **A)** Pictorial representation of Cetuximab-BPD (Cet-BPD) structure and switch mechanism based on lysosomal degradation and quenching of BPD molecules for tumor-targeted activatable photoimmunotherapy (taPIT). **B)** An illustrative comparison of the tumor-focused phototoxicity of taPIT vs non-specific action of perennially activated agents. Adapted from Spring *et al.*<sup>11</sup>

Overexpression of the EGFR has been observed in up to 70% of OvCa cases and is a biomarker for poor patient prognosis. This tumor-targeted and cell-activatable PIC relied on the static quenching of the BPD molecules whilst the PIC remained intact (OFF-state).<sup>11</sup> Following tumor cell binding, receptor-mediated endocytosis and subsequent intracellular endolysosomal degradation of the antibody, the BPD molecules were dequenched and activated (ON-state). This approach greatly simplifies dosimetry and helps reduce bowel toxicity, a major limitation to peritoneal PDT in the clinic. As the ultimate test for the PIC's tumor selectivity, a disseminated

micrometastatic OvCa *in vivo* model was used. Confocal microscopy demonstrated the PIC's capacity for EGFR selectivity through an 81% preferential localization of the PIC in epithelial OvCa cells over normal endothelial cells. Furthermore, a clinically used cisplatin/taxol combination produced only a modest 50% reduction in tumor burden after two rounds of chemotherapy, likely due to the chemoresistance of OvCa cells. In contrast, PDT using the Cet-BPD PIC resulted in 89% reduction in tumor burden. The combination of PIC-mediated PDT (1 cycle) with chemotherapy (1 cycle) resulted in an exceptional 97% reduction of peritoneal micrometastatic burden.

In addition to full-length antibody PICs, PSs have been conjugated to various smaller antibody fragments.<sup>194, 213-215</sup> Single-domain antibodies (SDAs), are approximately 10-times smaller than full-length antibodies and thus, faster physiological clearance rates mean that SDA- PICs can reach maximal tumor-to-normal ratios faster than larger PICs. Heuker *et al.* functionalized two EGFR-targeting SDAs with a silicon phthalocyanine PS derivative (IRDye® 700DX).<sup>216</sup> Both monovalent (non-internalizing) and bivalent (internalizing) SDAs were derivatized with the PS to investigate the dependence of cellular internalization on efficacy. Selectivity of cellular uptake and phototoxicity was determined in four cell lines with varying EGFR expression levels. In phototoxicity studies, the bivalent SDA-PIC was more potent, which is consistent with the general observation that intracellular PIC-mediated PDT is more effective. A phototoxicity study in a co-culture of 14C cells (high EGFR) and HeLa cells (low EGFR) using both SDA-PICs showed an EGFR-selective reduction in viability in the 14C cells. However, the rate of the phototoxicity of the bivalent internalizing SDA-PIC was significantly higher than that of the monovalent non-internalizing SDA-PICs.

The field of PICs has shown tremendous promise in cancer therapy and diagnostics and there has been a marked rise in the number of PIC studies reporting their effectiveness as targeted molecular imaging probes and PS conjugates that are selective to the tumor and components of the tumor stroma.<sup>184, 201, 205, 217, 218</sup> However, the clinical translation of PICs has lagged behind their ADC counterparts. Other challenges in PIC such as stability, clearance, tumor penetration and toxicity are common to ADCs and biological therapeutics. Specifically for PDT, complex light dosimetry parameters need to be further tackled with novel PIC and agent delivery strategies. None-the-less, an active clinical trial supported by Aspyrian Therapeutics, Inc.<sup>TM</sup> is currently recruiting for EGFR-selective PIT in patients with recurrent head and neck cancers.<sup>219</sup> Such exciting initiatives motivate a further drive in expanding PICs as precursors to targeted PNM formulations, whereby the long-standing preclinical efficacy of PIT is further advanced through nanotechnology.

#### Targeted nanotherapeutics as mediators for selectivity

As discussed previously, nanocarriers that are passively targeted to tumor tissue hold significant benefits over the use of free pharmaceutical agents, particularly when the drug freely escape from the carrier or can exert its effect whilst still encapsulated. However, many agents with intracellular targets are unable to diffuse across membranes freely. Conjugation of small molecules, peptides, or antibodies onto the carrier surface may potentiate cell-particle interactions, leading to enhanced uptake and intracellular accumulation of the drug. There is a wide variety of ligands used to target nanocarriers to cancer tissue, which includes folate,<sup>220</sup> RGD peptides,<sup>221</sup> full-length antibodies,<sup>53</sup> Fab' fragments,<sup>222</sup> and single domain antibodies.<sup>223</sup> Depending on the PKs of the nanoconstruct, it should be emphasized that ligand-targeted nanotherapeutics does not always improve drug delivery to the target site in comparison to untargeted nanocarriers, but has the benefit of facilitating selective cellular uptake to improve drug efficacy and treatment response.<sup>53</sup> However, nanoparticle targeting may also be achieved without the use of conjugated targeting ligands. For instance, liposomes carrying a positive surface charge are taken up specifically by angiogenic endothelial cells, and can thus be used to specifically target the tumor vasculature.<sup>224-226</sup> As cationic liposomes can interact with the cell membrane, it is thought that the distorted blood flow at the tumor site leads to shedding of the barrier-forming glycocalyx on endothelial cells and thus, increases the potential for liposome-cell membrane interaction.<sup>225-227</sup> Although a plethora of different cationic nanocarriers have shown potential as drug delivery systems, it is currently unclear whether all cationic nanoparticles exert selectivity for the tumor vasculature or whether this phenomenon is specific for liposomes.<sup>227</sup>

In the field of PDT, targeted PNM formulations may be instrumental in achieving higher vascular selectivity of the treatment. As an advancement to PICs with the additional capacity to selectively deliver high payloads of co-encapsulated secondary agents, targeted PNM formulations hold significant potential in future clinical applications of PDT. However, targeted nanocarriers for PDT have not been explored to a great extent. Targeted nanocarriers developed for PDT applications include gold, silica and polymeric nanoparticles functionalized with anti-HER2 antibodies, lectins (targeted to oncofetal glycans), anti-EGFR antibodies, folate molecules, a tumor vascular targeting F3 peptide and mannose.<sup>228-233</sup> All these targeted PNM platforms have enabled selective cancer cell uptake and have enhanced the PDT efficacies (Figure 12).

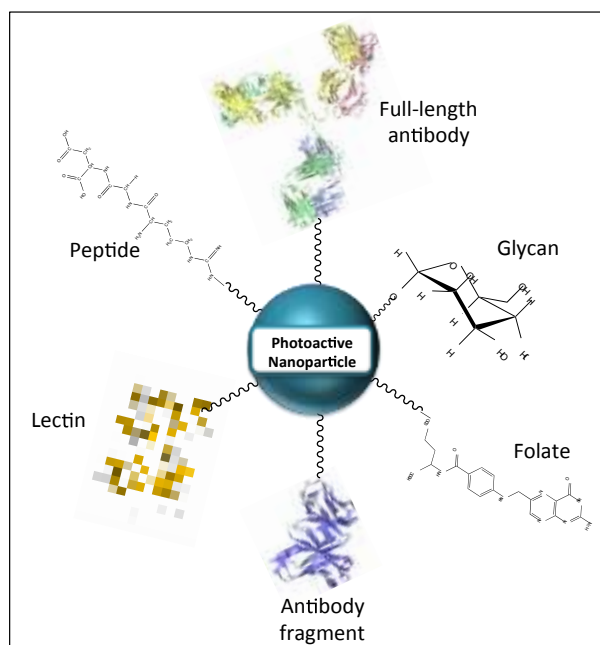


**Figure 12.** A diagrammatic representation of the different targeting ligands used to functionalize nanotherapeutics carrying PSs, to mediate the molecular selectivity of PDT damage. These include antibodies and antibody fragments, glycans targeting endogenous cell surface lectins, exogenous lectins targeting cell surface glycans, and folate molecules targeting the folate receptor.

With regards to liposomes, targeting of both hydrophobic and hydrophilic PSs has been explored with liposomal PSs conjugated to transferrin (sulfonated aluminum phthalocyanine), Uro-10 IgG antibodies (pyropheophorbide) and Cetuximab (BPD).<sup>234-236</sup> However, selective *in vivo* PDT using these targeted PNM formulations have yet to be fully investigated *in vivo*. The application of a BPD-containing liposomal formulation targeted to the neoangiogenic tumor vasculature by the conjugation of a custom APRPG peptide has been investigated *in vivo*. The results did not show enhanced tumor localization of BPD in comparison to non-targeted BPD-liposomes, yet targeted PDT yielded a 3-fold increase in efficacy.<sup>237</sup> The findings emphasize the importance of spatial control of damage and the necessity for targeted PNM formulations.

With respect to theranostic applications of targeted PNM formulations, silica nanoparticles containing both gadolinium and the PS Ce6 that were targeted with mannose were successfully developed and tested in a rat glioma model.<sup>238</sup> Similarly, polyacrylamide nanoparticles with entrapped porfimer sodium and the MRI contrast agent iron oxide that were functionalized with the nucleolin-binding peptide F3.<sup>239</sup> The targeted nanoparticles were shown to substantially enhance the selectivity of PDT on human MBA-MB-435 breast cancer cells *in vitro* by more than 80%, compared to therapy using non-targeted nanoparticles. Another interesting development in targeted PNM formulations is the progression of the aforementioned porphyrin structure that was used primarily for PTT.<sup>138</sup> Jin *et al.* used folate-derivatized porphyrins, where the lipidated pyropheophorbide PS molecules that were 99.1% quenched became destabilized and dequenched following *in vivo* targeting. The

targeted porphyrins bound to the folate-overexpressing KB tumors and subsequent cellular internalization resulted in the recovery of the lipidated PS's photoactivity.<sup>233</sup> Thus, targeting lead to effective PDT-mediated tumor photosensitization and a 6-fold inhibition in tumor growth, as compared to the non-targeted counterpart. Such exciting studies utilizing advanced PNM formulations for the targeted, tumor-specific induction of PDT are paving the way for further investigations in multiplexed PNM formulation-based combinatorial cancer therapy that will be discussed in the *Enhancing combination therapies using photonanomedicine* section.

## Approaches to manipulate cancer tissue using photochemistry and nanotechnology

### Effects and manipulation at the molecular and cellular level

In recent years, the biological responses of PDT have increasingly gained more attention. This information has led to a better understanding on the cell death mechanisms induced by various forms of PDT, as well the compensatory molecular phenomena that occur in the target tissue in its attempt to escape the treatment. It is becoming more evident that the most effective therapies for complicated cancers will involve multi-faceted combination treatments. Figure 13 is a conceptual diagram representing the mechanisms of RMS-mediated tumor damage induced by PDT and how the knowledge of pro-survival molecular pathways induced by an initial therapy can inform synergistic secondary treatment regimens to enhance the efficacy of PDT.

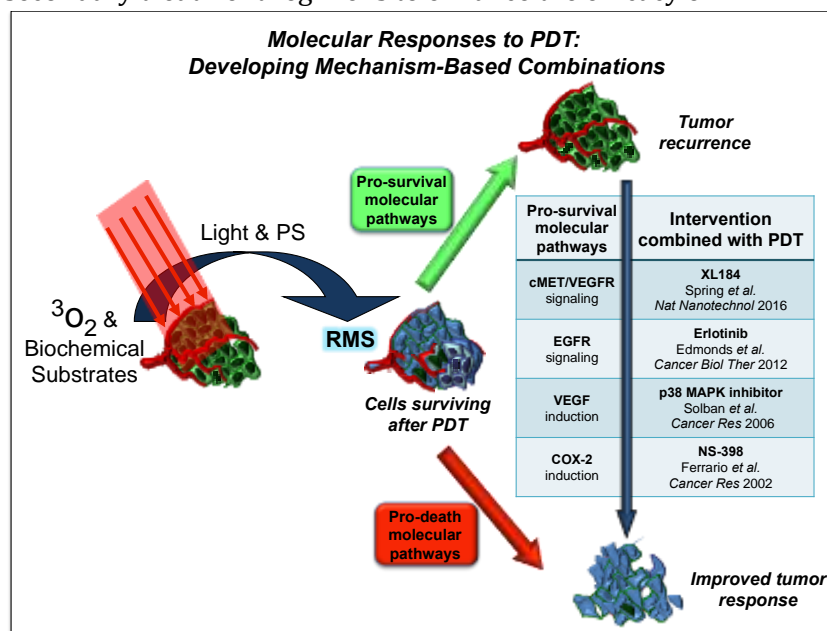


**Figure 13.** A conceptual depiction of the molecular responses to PDT and the rationale for mechanism-based combinations. PDT, like other mono-therapies, successfully kills a proportion of cancer cells while others survive. During the process of dying or injury, the cells mount a variety of pro-survival molecular responses that help the injured cells survive and the surviving cells proliferate. The figure gives only some examples of these pro-survival pathways/molecules that are secreted, upregulated or activated as a process of the “shock” of the PDT process. The pro-survival molecular responses elicited by the residual cancer cells following therapy require additional interventions, which can be intelligently co-delivered to the tumors using technologies such as theranostic PNM formulations. A strong, fundamental mechanistic justification for the selected combination maximizes the synergistic therapeutic effect, whilst minimizing toxicities. Examples of pro-survival molecular responses targeted in combination therapy with PDT include c-MET/VEGFR-2 signaling using the inhibitor XL184,<sup>51</sup> EGFR signaling using the inhibitor erlotinib,<sup>240</sup> VEGF induction using a p38 MAPK inhibitor<sup>241</sup> and cyclooxygenase-2 (COX-2) induction using the inhibitor NS-389.<sup>242</sup>

Numerous preclinical studies have already shown that PDT can synergize with chemotherapies and biological inhibitors, as well as re-sensitizing cancer cells to other therapeutic modalities. We strongly believe that designing PDT-based combination regimens that target multiple non-overlapping pathways, such that each component enhances the others, will most effectively improve the outcomes while minimizing systemic toxicities. In this

section, we will shortly review the cell death mechanisms induced by PDT, discuss the survival and growth strategies tumors engage to survive PDT, and how these mechanisms can be exploited to enhance the efficacy of anti-cancer treatments. This information will be of vital importance in the design and application of novel PNM formulations that can deliver mechanism-based combination therapies to synergistically improve treatment outcome. PS excitation leads to the production of highly oxidative RMS with short diffusion ranges. Specifically,  $^1\text{O}_2$  has an area of action that is limited to a spherical radius of diffusion of 100 nm.<sup>243</sup> Thus, the PDT effect is highly dependent on the intracellular localization of the PS.<sup>160</sup>

Hydrophobic PSs that reside within the lipid bilayer of the plasma membrane, for example porphyrin sodium and phthalocyanines,<sup>61</sup> are capable of oxidizing unsaturated fatty acids within the membrane, causing lipid packing defects that may culminate in necrosis. PSs that localize at the mitochondria, such as BPD,<sup>61</sup> may do the same for the mitochondrial membranes, resulting in mitochondrial membrane permeabilization and the release of apoptogenic factors.<sup>244</sup> Moreover, the mitochondrial membranes are replete with anti-apoptotic BCL2-family proteins, which are oxidized by the PDT-produced RMS, resulting in their dysfunction and prolongation of the apoptotic pathway.<sup>245</sup> Other prominent intracellular PS accumulation sites are the endoplasmic reticulum (ER) and the Golgi-apparatus.<sup>61</sup> Following PDT, the damage to these organelles induces ER-stress, protein aggregation, uncoupling of the intracellular  $\text{Ca}^{2+}$  homeostasis, and apoptosis *via* both mitochondrial-dependent and independent pathways.<sup>246, 247</sup> Lysosomal PSs exert their effects through lysosomal rupture, of which the released cathepsins are capable of relaying pro-apoptotic signaling, culminating in mitochondrial membrane permeabilization and apoptosis.<sup>248, 249</sup> However, when tumors are exposed to sublethal oxidative damage as a result of insufficient photosensitization or the inability of the excitation light to encompass the entire lesion, tumor cells activate coping mechanisms in their attempt to survive therapy. These survival mechanisms involve an antioxidant response, an inflammatory response, a hypoxic stress response, an immediate early response, and the ER-stress response, which have been elaborately reviewed.<sup>247</sup>

With the available knowledge on the cellular biological and molecular mechanisms by which PDT exerts its therapeutic effects, attempts have been made to enhance the therapeutic efficacy by using biomodulatory approaches to increase intracellular PS levels and to use adjuvant agents that block the PDT-related survival mechanisms. As these approaches entail multiple agents that may all have variable toxicities and individual PK profiles, the co-encapsulation of these agents into single PNM formulations may bear significant therapeutic potential.

For superficial tumors, PDT with the pro-PS ALA that is enzymatically converted into PpIX, is an effective treatment modality. Several biomodulatory approaches to increase the effect of ALA-PDT have focused on increasing PS accumulation in the tumor tissue. Vitamin D analogues calcitriol, cholecalciferol and calcipotriene have been shown to increase intracellular PpIX accumulation following ALA incubation,<sup>250, 251</sup> as a result of upregulated CCAAT enhancer binding protein  $\beta$  and coproporphyrinogen oxidase.<sup>252</sup> Similarly, methotrexate facilitates PpIX buildup in tumor cells by upregulating coproporphyrinogen oxidase and can exert additional chemotherapeutic effects by inhibiting DNA synthesis.<sup>253</sup> With these biomodulatory approaches, the intrinsic aberrant metabolic activity of tumor cells can be exploited using agents that are used clinically for a variety of pathologies. As both ALA and Vitamin D analogues are typically hydrophobic, their combined incorporation into a nanoparticle may be beneficial with respect to their plasma concentrations, PK behavior, cellular uptake, and synergistic effects on tumor photosensitization. With respect to survival pathway inhibition strategies, adjuvant therapies that prevent these survival pathways have yielded promising results. PDT's oxidative stress activates oxidation-sensitive activators of the NRF2 pathway that subsequently induces the transcription of genes that promote production of antioxidants such as glutathione. Hampering this antioxidant response using inhibitors of glutathione synthesis has been shown to be beneficial for the efficacy of PDT.<sup>254, 255</sup> With respect to hypoxia, the intratumoral depletion of oxygen is caused by its photochemical conversion into RMS, and is exacerbated by the vascular shutdown that ensues from PDT. The hypoxic tumor microenvironment activates hypoxia inducible factor

1, which stimulates anaerobic glycolysis, promotes angiogenesis and reduces sensitivity to cell death.<sup>256</sup> Interfering with these survival responses in combination with PDT has resulted in an enhancement of PDT efficacy in both *in vitro* and *in vivo* models of cancer.<sup>257-261</sup> In addition to the antioxidant and hypoxic stress responses, the ER-stress response is engaged as a result of massive protein oxidation and the consequential misfolding, unfolding and aggregation of the oxidized proteins.<sup>247, 262, 263</sup> Heat shock proteins and other chaperone proteins aid in the refolding or degradation of the oxidized polypeptides. Therefore, combining PDT with agents that prevent the execution of these chaperone-mediated survival mechanism have yielded promising results with respect to cell killing efficiency.<sup>263-265</sup> Studies during which PDT was combined with inhibitors of the inflammatory response and immediate early stress responses have yielded non-coherent results, potentially owing to the dichotomous functions of these signaling pathways with respect to cell survival and cell death.<sup>247, 266-268</sup>

At a molecular biological level, it is important to emphasize that PDT and more conventional cancer therapeutics, such as chemotherapy and RTs, do not have overlapping mechanisms of cytotoxicity. Classic chemotherapeutic agents and radiotherapy rely on inflicting DNA damage that translates into an apoptotic pathway *via* the nucleus<sup>269, 270</sup>. In comparison, PDT may either cause direct by directly permeabilizing the plasma membrane of tumor cells, or by inducing apoptotic signaling *via* organelle damage.<sup>244, 271, 272</sup> Rizvi *et al.* have shown that ovarian spheroids treated with BPD-PDT were hypersensitized to carboplatin.<sup>156</sup> Similar results have been obtained with different PSs and chemotherapeutic agents,<sup>155, 273, 274</sup> underscoring that PDT and chemotherapy may act synergistically to eradicate tumor tissue more effectively. Several approved chemotherapeutic agents encompass molecular inhibitors of pro-survival pathways that have been implicated in cellular resistance to PDT, such as bortezomib, an inhibitor of the ER-stress response. The findings summarized herein underline the potential of combination therapies to synergistically enhance cancer treatment outcomes, which can be potentiated by the co-encapsulation of both phototherapeutic and chemotherapeutic compounds into singular nanoparticulate formulations. However, it must be noted that PNM formulations not only alter PK and biodistribution profiles of PSs, but also govern their intracellular fate. Thus, manipulating tumor tissue as informed by the cellular effects of PDT using a particular PS may not be as effective when the biomodulatory agent and the same PDT agent are co-encapsulated into a single PNM formulation.

#### Enhancing combination therapies using photonanomedicine

Combination chemotherapy is the front line anti-cancer treatment regimen currently used in the clinic.<sup>275</sup> However, this approach based on the co-administration of two or more drugs, is far from ideal and suffers from varying bioavailability, PKs, bio-distribution and systemic toxicity.<sup>276</sup> These challenges have spurred the development of both organic and inorganic nanoparticles capable of delivering multiple chemotherapeutics and diagnostic agents.<sup>276-278</sup> These multi-agent delivery vehicles enable stoichiometric cargo loading, controlled delivery, prolonged circulation times and tumor targeting *via* the EPR effect. While these constructs have been reviewed elsewhere, here we focus on nanoparticle platforms that leverage light to employ mechanistically-informed therapeutic modalities at the 'right place and the right time'.

As discussed in the *Effects and manipulation at the molecular and cellular level* section, drug resistance mechanisms and escape pathways are a major hurdle to maximizing the therapeutic effects of drugs. In an effort to tackle these challenges, Spring *et al.* recently developed a multi-agent platform termed a photoactivatable multi-inhibitor nanoliposome (PMIL).<sup>51</sup> The PMIL is based on a core-shell architecture where a lipid layer embedded with hydrophobic BPD PS molecules encases a PEG-PLGA nanoparticle that entraps a secondary hydrophobic multi-kinase inhibitor, XL184 (cabozantinib, Cometriq®). The water soluble block copolymer nanoparticles were physically entrapped in BPD-containing photoactive lipid bilayers, and possibly monolayers that are known to self-assemble onto PLGA nanoparticles.<sup>279</sup> The PMIL platform combines three complimentary treatment modalities: PDT, VEGFR-2 receptor inhibition and c-MET receptor inhibition to elicit the anti-vascular and anti-tumoral properties of PDT with the anti-angiogenic and anti-invasive effects of XL184. Upon NIR light illumination, PDT damages tumor cells and induces thrombotic cascades that ultimately lead to vascular occlusion. It is speculated

that a macrophysiological effect, such as vascular occlusion, can lead to prolonged intratumoral retention of nanotherapeutics. The complex vascular effects of PDT and its specific role on the delivery of nanomedicines will be described in further detail in the *Manipulation at the macrophysiological level* section. The PMIL was designed to shield XL184-containing nanoparticles by the photoactive lipid encapsulation, until photoirradiation of the BPD PS with 690 nm light disrupts the lipid layer and triggers controlled release of the XL184. Subsequent slow-release biodegradable nanoparticles, such as the PEG-PLGA particle encapsulating the XL184, can be chemically tuned to modulate the drug release kinetics and sustain tumor exposure to the agent, thus presenting an additional layer of complexity to combinatorial PNM formulations such as the PMIL. XL184 inhibits VEGFR-2 and c-MET signaling, thus suppressing several escape pathways that govern tumor angiogenesis, vascular regrowth, tumor cell invasion and metastatic escape. This synergistic three-way mode of action elicited by PMIL-based combinatorial PDT is summarized in Figure 14.

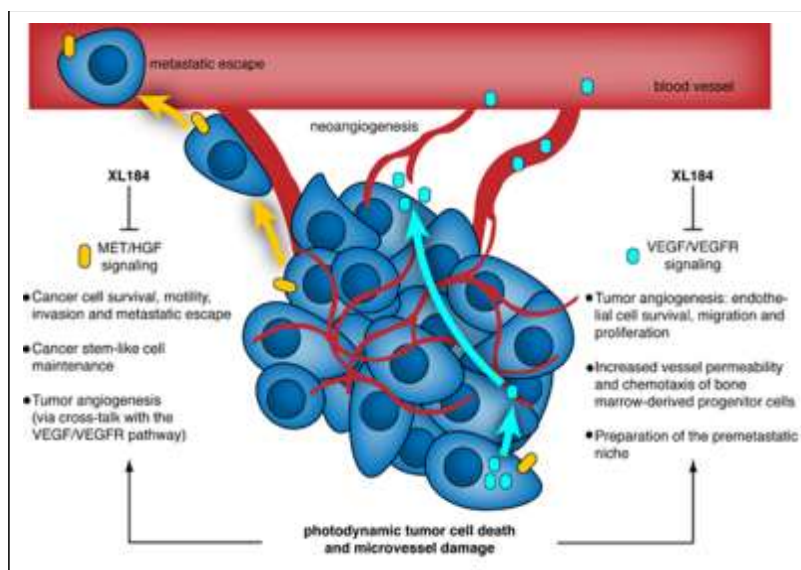


**Figure 14.** Schematic representation of the three-way mode of action of photoactivatable multi-inhibitor nanoliposomes (PMIL).<sup>51</sup>

In a subcutaneous mouse model of pancreatic cancer, combinatorial PDT using the PMIL reduced the mean tumor volume by 92% compared to the no-treatment control group, whilst the monotherapies and the co-administered same nanoformulations of BPD and XL184 packaged individually had no significant effect. Moreover, in an orthotopic metastatic pancreatic model, PMIL showed a reduction in microvasculature of the tumors and a 99% mean reduction in liver and retroperitoneal lymph node metastasis, with respect to the no-treatment control group. Interestingly the dosage of XL184 in the PMIL was 1000-fold lower than that used in standard oral preclinical regimens needed to achieve the same therapeutic efficacy. This increased drug potency underscores a substantial advantage of PNM formulations, considering the systemic toxicity of multi-kinase inhibitors like XL184. The light-assisted, controlled release of secondary agents such as XL184 from PNM formulations is critical to their improved tolerance. The improved efficacy of the PMIL is multi-factorial, owing to the fact that such PNM formulations improve bioavailability of therapeutics, increase tumor accumulation, prime and resensitize tumors to inhibitors through PDT and most importantly, provide a sophisticated platform for the spatiotemporal induction of multiple combined treatment regimes.

In a complimentary approach to overcome PDT escape pathways mediated by VEGF, Tangutoori *et al.* aimed to neutralize intracellular VEGF prior to its secretion.<sup>280</sup> To realize this goal, a nanophotoactivatable liposome (nanoPAL) platform was developed.<sup>280</sup> This multi-agent vehicle was loaded with BPD embedded in the liposomal bilayer and the clinically-approved anti-VEGF monoclonal antibody, bevacizumab (Avastin®), encapsulated in the aqueous core, for the photo-triggered intracellular delivery. The synthesis parameters were rigorously optimized to preserve the antibody's biological activity, to maintain BPD in its monomeric photoactive state, to offer

favorable payload release and to promote cellular uptake whilst limiting systemic toxicity through a moderate cationic surface charge. Figure 15 (A) shows the TEM images of the nanoPAL before and after PDT using 1 J/cm<sup>2</sup> of 690 nm light, which results in the destabilization of the spherical structure. Loss of liposomal integrity translates to the therapeutic phototriggered release of bevacizumab. *In vitro* studies using human pancreatic ductal adenocarcinoma cells (AsPC1) demonstrated that the integrated nanoPAL platform enhanced the cellular co-delivery of fluorescently labeled bevacizumab and BPD, as compared to the co-incubation of the individual liposomal BPD formulation, Visudyne®, and free bevacizumab. This trend was also observed in cytotoxicity studies in the same cell line, with nanoPAL eliciting 82% cell death relative to only 54% by the co-incubated independent agents upon light irradiation. Finally, in a subcutaneous AsPC1 xenograft model of pancreatic cancer, treatment with a co-administered regimen of independent Visudyne® and bevacizumab agents only stabilized tumor growth. In contrast, co-administration through the nanoPAL platform induced extensive necrotic tumor damage and arrested tumor growth. Minimal regrowth of the tumor was observed through completion of the study at 35 days.

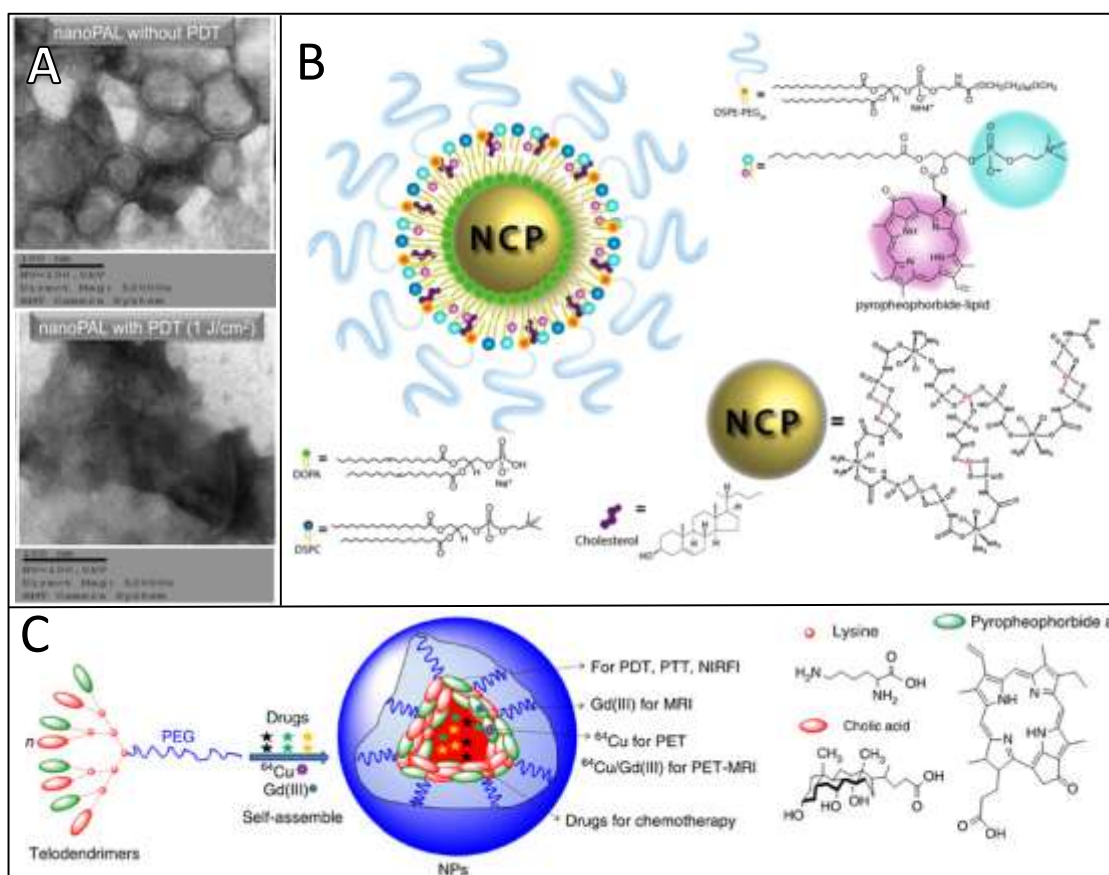


**Figure 15.** Multi-agent nanoconstructs for mechanistically informed combination therapy **A**) TEM images of nanophotoactivatable liposome (nanoPAL) before and after PDT. (Reprinted from Tangutoori *et al.*<sup>280</sup> with permission from Elsevier.) **B**) Pictorial representation of the structure and composition of the NCP@pyrolipid (Adapted with permission from He *et al.*<sup>281</sup> copyright 2015 American Chemical Society.) and **C**) the nanoporphyrin platform (NP) (Reprinted by permission of Macmillan Publishers Ltd. Li *et al.*<sup>282</sup> Nature Communications, copyright 2014).

In another rendition of the core-shell design, He *et al.* developed a multi-agent nanoparticle to deliver cisplatin and the PS pyropheophorbide (Figure 15 (B)).<sup>281</sup> The core was based on their previously established nanoscale coordination polymer (NCP) platform within which cisplatin was coordinated as a prodrug with Pt in the +IV oxidation state. The shell was composed of a lipid bilayer doped with a phospholipid-porphyrin amphiphile (pyrolipid), originally developed by Zheng and Lovell for the porphysome.<sup>138, 283, 284</sup> The self-assembled ~108 nm nanoparticle, termed NCP@pyrolipid, resulted in quenching of the lipidated porphyrin pyropheophorbide PS

molecules. *In vitro* studies demonstrated that efficient uptake of NCP@pyrolipid within SQ20B head and neck cancer cells occurred within 1 hour and gradually destabilized after 2 hours, as indicated by an increase in PS fluorescence. The cytotoxicity of NCP@pyrolipid was tested in cisplatin-sensitive and cisplatin-resistant cell lines. The particle showed a potent synergistic action between PDT and cisplatin, reducing the IC<sub>50</sub> values in the JSQ3 cisplatin-resistant head and neck cancer line from 13.33  $\mu\text{M}$  using free cisplatin to 1.21  $\mu\text{M}$  using NCP@pyrolipid PDT when irradiated at 690 nm. Encouraged by these *in vitro* studies, the authors investigated the NCP@pyrolipid efficacy in a cisplatin-resistant SQ20B subcutaneous xenograft mouse model. Combinatorial NCP@pyrolipid-PDT resulted in approximately 83% reduction in tumor volume, whilst controls including chemotherapy alone, PDT alone and NCP@pyrolipid without irradiation did not result in any tumor regression at the administered dose. An elegant micellar construct called Nanoporphyrin (NP) was introduced by Li *et al.* as an 'all-in-one' theranostic platform (Figure 15 (C)).<sup>282</sup> NP were based on linear PEG chains and a dendritic oligomer composed of the PS pyropheophorbide *a* and cholic acid. To improve stability in the blood, NPs were further stabilized by disulfide cross-linking. The incorporation of the PS within the delivery vehicle itself lies at the core of the NP design. The PS is quenched in the NP and activated upon NP dissociation *via* light activation and disulfide reduction in the tumor microenvironment, thus reducing non-specific off-target phototoxicity. Irradiation of the PS with NIR light generated RMS and localized thermalization to induce both PDT and PTT therapeutic modalities, respectively. Further, doxorubicin was also loaded into the hydrophobic core of the cross-linked NPs. The therapeutic efficacy of combined PDT, PTT and doxorubicin was successfully demonstrated in transgenic breast cancer and OvCa xenograft mouse models. The innate metal-chelating capability of NP enabled loading of Gd(III) and <sup>64</sup>Cu(II) for to provide theranostic PNM formulations that are capable of acting as contrast agents for MRI and PET imaging respectively, in addition to the NIR fluorescence imaging capabilities. NP's ability to detect tumors by NIR fluorescence imaging, MRI, PET as well as dual MRI-PET were demonstrated in multiple mouse models. Wang *et al.* engineered a dual-switch mesoporous silica nanoparticle (MSN) platform capable of selectively delivering drugs to either the extracellular or intracellular environment.<sup>285</sup> This was achieved by using two gates that trapped the cargo in the MSN pores, and opened upon either UV-light exposure or a decrease in pH levels. The switch mechanism was based on binding between  $\alpha$ -cyclodextrin with phenyl groups (pH responsive) and  $\beta$ -cyclodextrin with azobenzene groups (UV-responsive). The controlled dual-delivery was demonstrated with fluorescent dyes and the anti-cancer drugs octreotide acetate and epirubicin. Octreotide acetate elicits its cytotoxicity by binding to somatostatin receptors on the cell surface while epirubicin blocks DNA/RNA machinery in the nucleus. Cell viability assays using A549 cells demonstrated maximal efficacy of the dual-drug loaded MSNs with both UV and pH-activation, compared to either trigger alone. While this proof of concept study is encouraging, the applicability of UV light for deep tissue photoactivation is limited and potential long-term toxicity issues related to MSN administration need to be fully investigated.

#### Manipulation at the macrophysiological level

As discussed earlier in the *Tailoring tumor physiology to nanomedicines using photochemistry* section, low-dose vascular PDT (vPDT) can be used to enhance the delivery of nanomedicines by expanding the tumor vascular fenestrae, and thus further enhance the EPR effect. Within the context of therapeutic PDT tissue damage, the anti-tumor mechanisms of photochemistry include damaging the pathological vasculature, in addition to the aforementioned direct tumor cell insults.<sup>286</sup> vPDT relies on the preferential accumulation of the PS in the neovasculature over the tumor and is characterized by a short PS-light interval in its application, as shown in Figure 16.<sup>147, 286-289</sup>

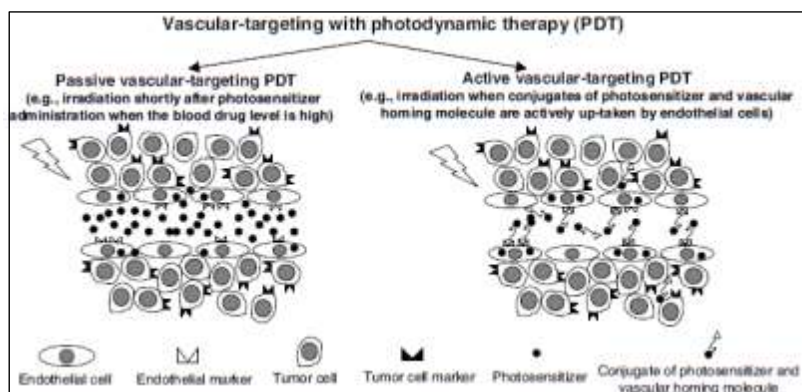


**Figure 16.** A Schematic representation of passive and active vascular PDT (vPDT).<sup>286</sup> Passive vPDT relies on the PS's inherent pharmacological ability to preferentially accumulate in the tumor vasculature while active vPDT leverages a tumor vascular homing ligand chemically conjugated to the PS or PS loaded nanoparticle. (Reproduced with permission of Begell House Inc. Publishers Chen *et al.*<sup>286</sup> Critical reviews in eukaryotic gene expression *via* the Copyright Clearance Center.)

High-dose vPDT causes thrombus formation, vasoconstriction, occlusion and decreased blood perfusion, whilst low-dose vPDT can be used to enhance vascular permeability. The most well known clinical application of high-dose vPDT has been for treating AMD with Visudyne®.<sup>290, 291</sup> In the anti-cancer arena TOOKAD has been widely studied as an intravascular PS for recurrent prostate cancer.<sup>147, 292</sup> vPDT can be achieved by either passive or active targeting. The former relies on the PK properties of the PS or the PNM formulation to preferentially accumulate in tumor vasculature within a specific time-period following intravenous injection, thus providing a therapeutic window.<sup>287, 293, 294</sup> Active targeting involves the conjugation of vasculature-specific ligands that selectively bind to proteins such as VEGFRs and integrins.<sup>286, 295</sup> In this section, nanoparticle-assisted vPDT by both passive and active targeting strategies will be the focus.

Different nanoparticle formulations used to deliver the same PS can result in cellular PDT, vPDT or a combination of both. In a study by Garcia-Diaz *et al.*, the PS temocene was delivered in three formats: micellar, liposomal and free form.<sup>296</sup> *In vivo* studies were performed as either vascular or cellular PDT using a 15 minute or 24 hour PS-light interval, respectively. Interestingly, the most effective treatment was observed in the case of temocene delivered in micelles with a short PS-light interval through vPDT, whilst liposomal temocene was more potent with the longer PS-light interval inducing cellular PDT. The Russell group developed surface functionalized gold nanoparticles with a zinc phthalocyanine-based PS.<sup>297</sup> PDT efficacy studies in a murine model of amelanotic melanoma were performed with a PS-light interval of 3 hours and 24 hours following injection of the nanoparticles, which correspond to the highest accumulation time points in the serum and the tumor, respectively. A delay in tumor regrowth was observed in the shorter interval treatment regimen, implying a more vPDT-based mechanism of action. This was conclusively demonstrated with electron microscopy images of tumor tissues that showed extensive capillary damage and leakage of erythrocytes.

Active targeting of nanoparticles to the tumor vasculature with peptide ligands is a promising complimentary strategy.<sup>232, 295</sup> A landmark study by Reddy *et al.* used Photofrin® encapsulated in polyacrylamide particles functionalized with the vascular homing, 31 residue F3 peptide.<sup>232</sup> The F3 peptide binds to the cell surface protein nucleolin, which is a marker for angiogenic endothelial cells in the tumor vasculature. Guided by MRI imaging through the integration of iron oxide within the PNM formulation, PDT treatment demonstrated higher survival rates in glioma-bearing rats treated with the targeted nanoparticles, as compared to non-targeted particles or un-encapsulated Photofrin®.

Recently, Bechet *et al.* developed a hybrid silica-based nanoparticle with encapsulated gadolinium oxide for MRI imaging and a chlorin PS for PDT.<sup>298, 299</sup> These ultra-small particles, approximately 2.8 nm in diameter, were surface-functionalized with a short peptide sequence (ATWLPPR) that targets tumor vasculature by binding to the VEGF receptor neuropilin-1 (NRP-1).<sup>300, 301</sup> Following *in vitro* validation of NRP-1 targeting and phototoxicity, the

multi-functional particles were used to treat glioblastoma multiforme in an orthotopic rat model. MRI imaging of the tumor tissue allowed real-time stereotactic interstitial PDT. Interestingly, the particles localized to the proliferating angiogenic endothelial cells lining the neovessels in the tumor periphery. Following interstitial PDT, multiple non-invasive imaging modalities such as perfusion MRI, proton magnetic resonance spectroscopy and PET-CT were employed to monitor the tumor status. Reduced blood perfusion rates, increased fatty acid production, as well as histological demonstration of vascular disruption and edema, proved a potent *in vivo* PDT effect.

As with most treatment modalities, more than one mode of action that unite and complement each other can provide significantly improved therapeutic outcomes. A unique advantage of PDT, and subsequent advanced PNM formulations developed thereof, that distinguish them from single modality treatment regimens, is their capacity for high spatiotemporal control over treatment induction, and therefore, mechanism of action. The combined effect of vascular and cellular PDT damage has thus far been achieved through the optimized PS-light interval; however, PNM formulations targeted towards both cellular and vascular tumor components further promise to enhance selectivity and control over PDT action.

### Summary and Prospective

Nanomedicine has progressed significantly in recent years because of the high surface area-to-volume ratio of nanoconstructs, their capacity for enhanced site-specific targeting, their capability for cell membrane internalization and their significant biocompatibility following breakthroughs in appropriate surface modifications. Numerous soft nanoconstructs have shown great promise for improving drug stability, altering PK and PD profiles, reducing systemic toxicity, and increasing drug concentrations at tumor site, while many are already approved for human clinical use. These soft nanoconstructs can be relatively easily modified with small photosensitizing molecules adding new functionality to existing FDA-approved nanomedicines. Exciting progress of inorganic 'hard' nanomedicines is promising in preclinical studies and clinical trials as therapeutics, whilst few are granted for medical imaging applications in humans. Many of these hard nanomedicines may already possess unique photoresponsive properties (*e.g.* the surface plasmon resonance properties of gold nanoconstructs) and have been intelligently combined with photosensitizing molecules. In addition to their photochemical therapeutic effects, these hard nanoparticles can image disease tissues *via* multiple non-invasive and minimally-invasive imaging methods, such as photoacoustic imaging, CT imaging and fluorescence imaging. These emerging imaging techniques have the potential to aid early diagnostics and treatment regimens with potential applications in detecting early-stage cancer, as well as in guiding drug delivery, light dosimetry, and even surgery. The ability to use photoactive nanomedicines as theranostic contrast agents has attracted increased attention, as they can overcome common drawbacks such as weak photostability, low sensitivity and physiological compatibility that are associated with traditional contrast agents.

In summary, the substantial chemical and optical advances in nanotechnology has led to a paradigm shift in the field of photomedicine. Although one of the early-approved nanotherapeutics was a PNM formulation (Visudyne®), there are relatively few PNM formulations for cancer in clinical studies compared to the number of PNM-related publications. In principle, these promising preclinical PNM formulations possess the ability to image malignant tissues and spatiotemporally control the release of chemical and biological therapeutic payloads, resensitizing tumor to the agents which they ultimately synergize with. Furthermore, the pre-clinical PNM formulations can also modulate tumor microenvironments to enhanced tumor delivery of drugs and nanoparticles. Much of this potential remains to be realized in complex systems prior to clinical translation but does offer exciting opportunities to further advance cancer theranostics. The true clinical impact of these advanced optical nanoplatfroms is expected in the coming decade as the convergence in the scientific and medical understanding of photomedicine and nanotechnology ultimately realizes the niche potential for such state-of-the-art PNM formulations.

### Acknowledgements

We thank Dr. Bryan Spring, Dr. Srivalleesha Mallidi and Dr. Akilan Palanisami for insightful discussions. The support of the National Institutes of Health Grants P01CA084203, R01CA156177, and R01CA160998 to T.H. is gratefully acknowledged. Financial support by the Bullock-Wellman Postdoctoral Fellowship # 223794 for G.O. and the MGH-Tosteson-Funds for Medical Discovery (FMD) Fellowship #224889 for H-C.H. is also gratefully acknowledged.

## References

1. <http://worldwide.espacenet.com>.
2. <https://clinicaltrials.gov>, search 'nanoparticles'.
3. Y. Barenholz, *J Controlled Release*, 2012, **160**, 117-134.
4. <https://clinicaltrials.gov>, search 'liposomes'.
5. <https://clinicaltrials.gov>.
6. B. W. Henderson and T. J. Dougherty, *Photochem. Photobiol.*, 1992, **55**, 145-157.
7. T. J. Dougherty, C. J. Gomer, B. W. Henderson, G. Jori, D. Kessel, M. Korbelik, J. Moan and Q. Peng, *J. Natl. Cancer Inst.*, 1998, **90**, 889-905.
8. V. R. Participants, *Retina (Philadelphia, Pa.)*, 2005, **25**, 119-134.
9. R. R. Anderson and J. A. Parrish, *J. Invest. Dermatol.*, 1981, **77**, 13-19.
10. S. Mallidi, B. Q. Spring, S. Chang, B. Vakoc and T. Hasan, *Cancer J.*, 2015, **21**, 194-205.
11. B. Q. Spring, A. O. Abu-Yousif, A. Palanisami, I. Rizvi, X. Zheng, Z. Mai, S. Anbil, R. B. Sears, L. B. Mensah, R. Goldschmidt, S. S. Erdem, E. Oliva and T. Hasan, *Proc. Natl. Acad. Sci. U. S. A.*, 2014, **111**, E933-942.
12. J. T. Elliott, A. V. Dsouza, S. C. Davis, J. D. Olson, K. D. Paulsen, D. W. Roberts and B. W. Pogue, *Biomed. Opt. Express*, 2015, **6**, 3765-3782.
13. B. W. Pogue, C. Sheng, J. Benevides, D. Forcione, B. Puricelli, N. Nishioka and T. Hasan, *J. Biomed. Opt.*, 2008, **13**, 034009.
14. M. T. Jarvi, M. S. Patterson and B. C. Wilson, *Biophys. J.*, 2012, **102**, 661-671.
15. R. M. Valentine, S. H. Ibbotson, C. T. Brown, K. Wood and H. Moseley, *Photochem. Photobiol.*, 2011, **87**, 242-249.
16. J. Zhao, M. Wallace and M. P. Melancon, *Nanomedicine (London, U. K.)*, 2014, **9**, 2041-2057.
17. X. Huang, I. H. El-Sayed, W. Qian and M. A. El-Sayed, *J. Am. Chem. Soc.*, 2006, **128**, 2115-2120.
18. <https://clinicaltrials.gov>, NCT01679470.
19. <https://clinicaltrials.gov>, NCT02680535.
20. J.-L. Boulnois, *Lasers Med. Sci.*, 1986, **1**, 47-66.
21. M. S. Patterson, B. C. Wilson and R. Graff, *Photochem. Photobiol.*, 1990, **51**, 343-349.
22. M. T. Huggett, M. Jermyn, A. Gillams, R. Illing, S. Mosse, M. Novelli, E. Kent, S. G. Bown, T. Hasan, B. W. Pogue and S. P. Pereira, *Br. J. Cancer*, 2014, **110**, 1698-1704.
23. M. L. Etheridge, S. A. Campbell, A. G. Erdman, C. L. Haynes, S. M. Wolf and J. McCullough, *Nanomedicine*, 2013, **9**, 1-14.
24. V. Weissig, T. K. Pettinger and N. Murdock, *Int. J. Nanomed.*, 2014, **9**, 4357-4373.
25. E. M. Pridgen, F. Alexis, T. T. Kuo, E. Levy-Nissenbaum, R. Karnik, R. S. Blumberg, R. Langer and O. C. Farokhzad, *Sci. Transl. Med.*, 2013, **5**, 213ra167.
26. Y. Barak, W. J. Heroman and T. H. Tezel, *Middle East Afr. J. Ophthalmol.*, 2012, **19**, 43-51.
27. K. Ichikawa, Y. Takeuchi, S. Yonezawa, T. Hikita, K. Kurohane, Y. Namba and N. Oku, *Cancer Lett.*, 2004, **205**, 39-48.
28. M. Jermyn, S. C. Davis, H. Dehghani, M. T. Huggett, T. Hasan, S. P. Pereira, S. G. Bown and B. W. Pogue, *Phys. Med. Biol.*, 2014, **59**, 1911-1921.
29. S. G. Bown, A. Z. Rogowska, D. E. Whitelaw, W. R. Lees, L. B. Lovat, P. Ripley, L. Jones, P. Wyld, A. Gillams and A. W. Hatfield, *Gut*, 2002, **50**, 549-557.

30. C. M. Moore, A. R. Azzouzi, E. Barret, A. Villers, G. H. Muir, N. J. Barber, S. Bott, J. Trachtenberg, N. Arumainayagam, B. Gaillac, C. Allen, A. Schertz and M. Emberton, *BJU Int.*, 2015, **116**, 888-896.
31. S. Krishnamurthy, S. K. Powers, P. Witmer and T. Brown, *Lasers Surg. Med.*, 2000, **27**, 224-234.
32. M. S. Eljamel, C. Goodman and H. Moseley, *Lasers Med. Sci.*, 2008, **23**, 361-367.
33. <https://clinicaltrials.gov>, NCT00617981.
34. <https://clinicaltrials.gov>; NCT02112656.
35. <http://investor.celsion.com/releasedetail.cfm?ReleaseID=737033>.
36. <http://investor.celsion.com/releasedetail.cfm?ReleaseID=897613>.
37. A. Wang-Gillam, C. P. Li, G. Bodoky, A. Dean, Y. S. Shan, G. Jameson, T. Macarulla, K. H. Lee, D. Cunningham, J. F. Blanc, R. A. Hubner, C. F. Chiu, G. Schwartzmann, J. T. Siveke, F. Braiteh, V. Moyo, B. Belanger, N. Dhindsa, E. Bayever, D. D. Von Hoff, L. T. Chen and N.-S. Group, *Lancet*, 2015, DOI: 10.1016/S0140-6736(15)00986-1.
38. <http://www.fda.gov/NewsEvents/Newsroom/PressAnnouncements/ucm468654.htm>.
39. V. P. Torchilin, *Nat. Rev. Drug Discov.*, 2005, **4**, 145-160.
40. <https://clinicaltrials.gov>, NCT00802945.
41. A. Awada, A. A. Garcia, S. Chan, G. H. Jerusalem, R. E. Coleman, M. T. Huizing, A. Mehdi, S. M. O'Reilly, J. T. Hamm, P. J. Barrett-Lee, V. Cocquyt, K. Sideras, D. E. Young, C. Zhao, Y. L. Chia, U. Hoch, A. L. Hannah, E. A. Perez and N.-S. Group, *Lancet Oncol.*, 2013, **14**, 1216-1225.
42. <https://clinicaltrials.gov>, NCT02312622.
43. <https://clinicaltrials.gov>, NCT00806156.
44. <https://clinicaltrials.gov>, NCT01492101.
45. <http://ir.nektar.com/releasedetail.cfm?ReleaseID=902141>.
46. C. Oerlemans, W. Bult, M. Bos, G. Storm, J. F. Nijsen and W. E. Hennink, *Pharm. Res.*, 2010, **27**, 2569-2589.
47. O. Sartor, *Urology*, 2003, **61**, 25-31.
48. M. W. Saif, *JOP*, 2013, **14**, 686-688.
49. J. E. Lancet, J. E. Cortes, D. E. Hogge, M. S. Tallman, T. J. Kovacsovic, L. E. Damon, R. Komrokji, S. R. Solomon, J. E. Kolitz, M. Cooper, A. M. Yeager, A. C. Louie and E. J. Feldman, *Blood*, 2014, **123**, 3239-3246.
50. <https://clinicaltrials.gov>, NCT01696084.
51. B. Q. Spring, R. B. Sears, L. K. Zheng, Z. Mai, R. Watanabe, M. E. Sherwood, D. A. Schoenfeld, B. W. Pogue, S. P. Pereira, E. Villa and T. Hasan, *Nat. Nanotechnol.*, 2016, **in press**.
52. S. W. Morton, M. J. Lee, Z. J. Deng, E. C. Dreaden, E. Siouve, K. E. Shopsowitz, N. J. Shah, M. B. Yaffe and P. T. Hammond, *Sci. Signaling*, 2014, **7**, ra44.
53. C. Mamot, R. Ritschard, A. Wicki, G. Stehle, T. Dieterle, L. Bubendorf, C. Hilker, S. Deuster, R. Herrmann and C. Rochlitz, *Lancet Oncol.*, 2012, **13**, 1234-1241.
54. *Cancer Discovery - Immunoliposomes Are Active in EGFR-Overexpressing Solid Tumors*, 2013, **3**, OF15.
55. <https://clinicaltrials.gov>, NCT02213744.
56. J. Hrkach, D. Von Hoff, M. Mukkaram Ali, E. Andrianova, J. Auer, T. Campbell, D. De Witt, M. Figa, M. Figueiredo, A. Horhota, S. Low, K. McDonnell, E. Peeke, B. Retnarajan, A. Sabnis, E. Schnipper, J. J. Song, Y. H. Song, J. Summa, D. Tompsett, G. Troiano, T. Van Geen Hoven, J. Wright, P. LoRusso, P. W. Kantoff, N. H. Bander, C. Sweeney, O. C. Farokhzad, R. Langer and S. Zale, *Sci. Transl. Med.*, 2012, **4**, 128ra139.
57. J. Cui, C. Li, W. Guo, Y. Li, C. Wang, L. Zhang, L. Zhang, Y. Hao and Y. Wang, *J. Controlled Release*, 2007, **118**, 204-215.
58. R. Steiner, in *Laser and IPL Technology in Dermatology and Aesthetic Medicine*, ed. S. K. Christian Raulin, Springer Science & Business Media, 2011, ch. 2. Laser-Tissue Interactions.
59. S. L. Jacques, *J. Biomed. Opt.*, 2010, **15**, 051608.

60. S. M. Hahn, D. L. Fraker, R. Mick, J. Metz, T. M. Busch, D. Smith, T. Zhu, C. Rodriguez, A. Dimofte, F. Spitz, M. Putt, S. C. Rubin, C. Menon, H. W. Wang, D. Shin, A. Yodh and E. Glatstein, *Clin. Cancer Res.*, 2006, **12**, 2517-2525.
61. A. E. O'Connor, W. M. Gallagher and A. T. Byrne, *Photochem. Photobiol.*, 2009, **85**, 1053-1074.
62. <http://www.accessdata.fda.gov/scripts/cdrh/cfdocs/cfTopic/pma/pma.cfm?num=p990048>.
63. <http://www.fda.gov/drugs/informationondrugs/approveddrugs/ucm468728.htm>.
64. <http://www.fda.gov/safety/medwatch/safetyinformation/ucm359951.htm>.
65. <http://www.fda.gov/aboutfda/centersoffices/officeofmedicalproductsandtobacco/cder/ucm278957.htm>.
66. <http://www.fda.gov/drugs/informationondrugs/approveddrugs/ucm340913.htm>.
67. <http://www.fda.gov/MedicalDevices/ProductsandMedicalProcedures/DeviceApprovalsandClearances/Recently-ApprovedDevices/ucm089780.htm>.
68. <http://www.accessdata.fda.gov/scripts/cdrh/cfdocs/cftopic/pma/pma.cfm?num=p020021>.
69. B. W. Pogue, J. T. Elliott, S. C. Kanick, S. C. Davis, K. S. Samkoe, E. V. Maytin, S. P. Pereira and T. Hasan, *Phys Med Biol*, 2016, **61**, R57-89.
70. A.-L. Bulin, C. Truillet, R. Chouikrat, F. Lux, C. Frochot, D. Amans, G. Ledoux, O. Tillement, P. Perriat, M. Barberi-Heyob and C. Dujardin, *J. Phys. Chem. C*, 2013, **117**, 21583-21589.
71. G. Chen, H. Qiu, P. N. Prasad and X. Chen, *Chem. Rev.*, 2014, **114**, 5161-5214.
72. B. Kosharsky, N. Solban, S. K. Chang, I. Rizvi, Y. Chang and T. Hasan, *Cancer Res.*, 2006, **66**, 10953-10958.
73. M. Triesscheijn, P. Baas, J. H. Schellens and F. A. Stewart, *Oncologist*, 2006, **11**, 1034-1044.
74. A. C. Miller and B. W. Henderson, *Radiat. Res.*, 1986, **107**, 83-94.
75. <http://www.health.alberta.ca/documents/AHTDP-PDT-EEC-UofA-STE.pdf>.
76. S. Mura and P. Couvreur, *Adv. Drug Delivery Rev.*, 2012, **64**, 1394-1416.
77. M. J. Niedre, A. J. Secord, M. S. Patterson and B. C. Wilson, *Cancer Res.*, 2003, **63**, 7986-7994.
78. S. Mallidi, S. Anbil, S. Lee, D. Manstein, S. Elrington, G. Kositratna, D. Schoenfeld, B. Pogue, S. J. Davis and T. Hasan, *J. Biomed. Opt.*, 2014, **19**, 028001.
79. J. R. Mansfield, K. W. Gossage, C. C. Hoyt and R. M. Levenson, *J. Biomed. Opt.*, 2005, **10**, 9.
80. T. Zimmermann, J. Rietdorf and R. Pepperkok, *FEBS Lett.*, 2003, **546**, 87-92.
81. Q. T. Nguyen and R. Y. Tsien, *Nat. Rev. Cancer*, 2013, **13**, 653-662.
82. W. Stummer, H. J. Reulen, A. Novotny, H. Stepp and J. C. Tonn, in *Local therapies for glioma; Present status and future developments*, eds. M. Westphal, J. C. Tonn and Z. Ram, Springer-Verlag Wien KG, Sachsenplatz 4-6, A-1200, Vienna, Austria; Springer-Verlag New York Inc., 175 Fifth Avenue, New York, NY, 10010-7858, USA, 2003, vol. Volume 88, pp. 9-12.
83. G. Widhalm, S. Wolfsberger, G. Minchev, A. Woehrer, M. Krssak, T. Czech, D. Prayer, S. Asenbaum, J. A. Hainfellner and E. Knosp, *Cancer*, 2010, **116**, 1545-1552.
84. W. Stummer, U. Pichlmeier, T. Meinel, O. D. Wiestler, F. Zanella, R. Hans-Jurgen and G. Ala-Glioma Study, *Lancet Oncol.*, 2006, **7**, 392-401.
85. H. Kostron, in *Photodynamic Therapy: Methods and Protocols*, ed. C. J. Gomer, Humana Press Inc, Totowa, 2010, vol. 635, pp. 261-280.
86. D. Jocham, H. Stepp and R. Waidelich, *Eur. Urol.*, 2008, **53**, 1138-1150.
87. W. Zhong, J. P. Celli, I. Rizvi, Z. Mai, B. Q. Spring, S. H. Yun and T. Hasan, *Br. J. Cancer*, 2009, **101**, 2015-2022.
88. G. M. van Dam, G. Themelis, L. M. Crane, N. J. Harlaar, R. G. Pleijhuis, W. Kelder, A. Sarantopoulos, J. S. de Jong, H. J. Arts, A. G. van der Zee, J. Bart, P. S. Low and V. Ntziachristos, *Nat. Med.*, 2011, **17**, 1315-1319.
89. A. Palumbo, F. Hauler, P. Dziunycz, K. Schwager, A. Soltermann, F. Pretto, C. Alonso, G. F. Hofbauer, R. W. Boyle and D. Neri, *Br. J. Cancer*, 2011, **104**, 1106-1115.

90. E. Blanco, C. W. Kessinger, B. D. Sumer and J. Gao, *Exp. Biol. Med.*, 2009, **234**, 123-131.
91. J. E. Lee, N. Lee, T. Kim, J. Kim and T. Hyeon, *Acc. Chem. Res.*, 2011, **44**, 893-902.
92. W. X. Mai and H. Meng, *Integr. Biol.*, 2013, **5**, 19-28.
93. Y. Chen, H. R. Chen and J. L. Shi, *Adv. Mater.*, 2013, **25**, 3144-3176.
94. W. T. Al-Jamal and K. Kostarelos, *Acc. Chem. Res.*, 2011, **44**, 1094-1104.
95. R. Savla, O. Taratula, O. Garbuzenko and T. Minko, *J Controlled Release*, 2011, **153**, 16-22.
96. T. A. Zdobnova, O. A. Stremovskiy, E. N. Lebedenko and S. M. Deyev, *PLoS One*, 2012, **7**, 8.
97. K. Yang, L. Z. Feng, X. Z. Shi and Z. Liu, *Chem. Soc. Rev.*, 2013, **42**, 530-547.
98. C. G. Hadjipanayis, R. Machaidze, M. Kaluzova, L. Y. Wang, A. J. Schuette, H. W. Chen, X. Y. Wu and H. Mao, *Cancer Res.*, 2010, **70**, 6303-6312.
99. D. Ho, X. L. Sun and S. H. Sun, *Acc. Chem. Res.*, 2011, **44**, 875-882.
100. J. R. McCarthy and R. Weissleder, *Adv. Drug Delivery Rev.*, 2008, **60**, 1241-1251.
101. J. F. Hainfeld, D. N. Slatkin, T. M. Focella and H. M. Smilowitz, *Br. J. Radiol.*, 2006, **79**, 248-253.
102. L. A. Lane, X. M. Qian and S. M. Nie, *Chem. Rev.*, 2015, **115**, 10489-10529.
103. J. F. Hainfeld, D. N. Slatkin and H. M. Smilowitz, *Phys. Med. Biol.*, 2004, **49**, N309-N315.
104. M. Misawa and J. Takahashi, *Nanomedicine*, 2011, **7**, 604-614.
105. M. E. Wieder, D. C. Hone, M. J. Cook, M. M. Handsley, J. Gavrilovic and D. A. Russell, *Photochemical & photobiological sciences : Official journal of the European Photochemistry Association and the European Society for Photobiology*, 2006, **5**, 727-734.
106. L. Dykman and N. Khlebtsov, *Chem. Soc. Rev.*, 2012, **41**, 2256-2282.
107. L. Sancey, F. Lux, S. Kotb, S. Roux, S. Dufort, A. Bianchi, Y. Cremillieux, P. Fries, J. L. Coll, C. Rodriguez-Lafresse, M. Janier, M. Dutreix, M. Barberi-Heyob, F. Boschetti, F. Denat, C. Louis, E. Porcel, S. Lacombe, G. Le Duc, E. Deutsch, J. L. Perfettini, A. Detappe, C. Verry, R. Berbeco, K. T. Butterworth, S. J. McMahon, K. M. Prise, P. Perriat and O. Tillement, *Br. J. Radiol.*, 2014, **87**, 15.
108. S. Mallidi, H.-C. Huang, J. Y. Liu, L. Mensah, Z. Mai and T. Hasan, *Cancer Research*, 2013, **73**, 3923.
109. C. J. Ho, G. Balasundaram, W. Driessen, R. McLaren, C. L. Wong, U. S. Dinish, A. B. Attia, V. Ntziachristos and M. Olivo, *Sci. Rep.*, 2014, **4**, 5342.
110. Y. Chen, M. Sajjad, Y. Wang, C. Batt, H. A. Nabi and R. K. Pandey, *ACS Med. Chem. Lett.*, 2011, **2**, 136-141.
111. S. Mallidi, K. Watanabe, D. Timerman, D. Schoenfeld and T. Hasan, *Theranostics*, 2015, **5**, 289-301.
112. J. E. Rosen, Y. Serge, M. Ameena, V. Mohit and X. G. Frank, *J. Nanomed. Nanotechnol.*, 2011, **2**, 1000115.
113. J. T. Elliott, K. S. Samkoe, J. R. Gunn, E. E. Stewart, T. B. Gardner, K. M. Tichauer, T. Y. Lee, P. J. Hoopes, S. P. Pereira, T. Hasan and B. W. Pogue, *Acad. Radiol.*, 2015, **22**, 572-579.
114. K. Tanha, A. M. Pashazadeh and B. W. Pogue, *Biomed. Opt. Express*, 2015, **6**, 3053-3065.
115. R. X. Zhang, A. V. D'Souza, J. R. Gunn, T. V. Esipova, S. A. Vinogradov, A. K. Glaser, L. A. Jarvis, D. J. Gladstone and B. W. Pogue, *Opt. Lett.*, 2015, **40**, 827-830.
116. J. Axelsson, S. C. Davis, D. J. Gladstone and B. W. Pogue, *Med. Phys.*, 2011, **38**, 4127-4132.
117. L. A. Jarvis, R. X. Zhang, D. J. Gladstone, S. D. Jiang, W. Hitchcock, O. D. Friedman, A. K. Glaser, M. Jermyn and B. W. Pogue, *Int. J. Radiat. Oncol., Biol., Phys.*, 2014, **89**, 615-622.
118. H. H. Ross, *Anal. Chem.*, 1969, **41**, 1260-1265.
119. N. Kotagiri, G. P. Sudlow, W. J. Akers and S. Achilefu, *Nat. Nanotechnol.*, 2015, **10**, 370-379.
120. M. Silindir, A. Y. Ozer and S. Erdogan, *Drug Delivery*, 2012, **19**, 68-80.
121. W. Chen and J. Zhang, *J. Nanosci. Nanotechnol.*, 2006, **6**, 1159-1166.
122. E. L. Rosenthal, J. M. Warram, E. de Boer, T. K. Chung, M. L. Korb, M. Brandwein-Gensler, T. V. Strong, C. E. Schmalbach, A. B. Morlandt, G. Agarwal, Y. E. Hartman, W. R. Carroll, J. S. Richman, L. K. Clemons, L. M. Nabell and K. R. Zinn, *Clin. Cancer Res.*, 2015, **21**, 3658-3666.
123. A. C. Anselmo and S. Mitragotri, *AAPS J.*, 2015, **17**, 1041-1054.
124. E. Reddi, G. Lo Castro, R. Biolo and G. Jori, *Br. J. Cancer*, 1987, **56**, 597-600.
125. M. E. Davis, Z. Chen and D. M. Shin, *Nat. Rev. Drug Discov.*, 2008, **7**, 771-782.

126. L. Li and K. M. Huh, *Biomater. Res.*, 2014, **18**, 19.
127. A. M. Richter, E. Waterfield, A. K. Jain, A. J. Canaan, B. A. Allison and J. G. Levy, *Photochem. Photobiol.*, 1993, **57**, 1000-1006.
128. Z.-J. Wang, Y.-Y. He, C.-G. Huang, J.-S. Huang, Y.-C. Huang, J.-Y. An, Y. Gu and L.-J. Jiang, *Photochem. Photobiol.*, 1999, **70**, 773-780.
129. N. Oku, N. Saito, Y. Namba, H. Tsukada, D. Dolphin and S. Okada, *Biol. Pharm. Bull.*, 1997, **20**, 670-673.
130. C. Milanese, R. Biolo, E. Reddi and G. Jori, *Photochem. Photobiol.*, 1987, **46**, 675-681.
131. V. Reshetov, H. P. Lassalle, A. Francois, D. Dumas, S. Hupont, S. Grafe, V. Filipe, W. Jiskoot, F. Guillemain, V. Zorin and L. Bezdetnaya, *Int. J. Nanomed.*, 2013, **8**, 3817-3831.
132. J. Buchholz, B. Kaser-Hotz, T. Khan, C. Rohrer Bley, K. Melzer, R. A. Schwendener, M. Roos and H. Walt, *Clin. Cancer Res.*, 2005, **11**, 7538-7544.
133. Z. J. Wang, Y. Y. He, C. G. Huang, J. S. Huang, Y. C. Huang, J. Y. An, Y. Gu and L. J. Jiang, *Photochem. Photobiol.*, 1999, **70**, 773-780.
134. J. O'Hara, K. S. Samkoe, A. Chen, P. J. Hoopes, I. Rizvi, T. Hasan and B. W. Pogue, 2009.
135. H. Maeda, *Adv. Enzyme Regul.*, 2001, **41**, 189-207.
136. H. Maeda, *Bioconjugate Chem.*, 2010, **21**, 797-802.
137. A. Gabizon, R. Catane, B. Uziely, B. Kaufman, T. Safra, R. Cohen, F. Martin, A. Huang and Y. Barenholz, *Cancer Res.*, 1994, **54**, 987-992.
138. J. F. Lovell, C. S. Jin, E. Huynh, H. Jin, C. Kim, J. L. Rubinstein, W. C. Chan, W. Cao, L. V. Wang and G. Zheng, *Nat. Mater.*, 2011, **10**, 324-332.
139. D. Liu, A. Mori and L. Huang, *Biochim. Biophys. Acta, Biomembr.*, 1992, **1104**, 95-101.
140. V. D. Awasthi, D. Garcia, B. A. Goins and W. T. Phillips, *Int. J. Pharm.*, 2003, **253**, 121-132.
141. H. Hashizume, P. Baluk, S. Morikawa, J. W. McLean, G. Thurston, S. Roberge, R. K. Jain and D. M. McDonald, *Am. J. Pathol.*, 2000, **156**, 1363-1380.
142. D. C. Drummond, O. Meyer, K. Hong, D. B. Kirpotin and D. Papahadjopoulos, *Pharmacol. Rev.*, 1999, **51**, 691-744.
143. U. Prabhakar, H. Maeda, R. K. Jain, E. M. Sevick-Muraca, W. Zamboni, O. C. Farokhzad, S. T. Barry, A. Gabizon, P. Grodzinski and D. C. Blakey, *Cancer Res.*, 2013, **73**, 2412-2417.
144. V. P. Chauhan, T. Stylianopoulos, J. D. Martin, Z. Popović, O. Chen, W. S. Kamoun, M. G. Bawendi, D. Fukumura and R. K. Jain, *Nat. Nanotechnol.*, 2012, **7**, 383-388.
145. R. K. Jain, *Nat. Med.*, 2001, **7**, 987-989.
146. B. W. Henderson, S. M. Waldow, T. S. Mang, W. R. Potter, P. B. Malone and T. J. Dougherty, *Cancer Res.*, 1985, **45**, 572-576.
147. B. Chen, B. W. Pogue, J. M. Luna, R. L. Hardman, P. J. Hoopes and T. Hasan, *Clin. Cancer Res.*, 2006, **12**, 917-923.
148. H. Kobayashi, R. Watanabe and P. L. Choyke, *Theranostics*, 2013, **4**, 81-89.
149. J. W. Snyder, W. R. Greco, D. A. Bellnier, L. Vaughan and B. W. Henderson, *Cancer Res.*, 2003, **63**, 8126-8131.
150. Y. Wang, M. Gonzalez, C. Cheng, A. Haouala, T. Krueger, S. Peters, L. A. Decosterd, H. van den Bergh, J. Y. Perentes, H. B. Ris, I. Letovanec and E. Debeve, *Lasers Surg. Med.*, 2012, **44**, 318-324.
151. Z. Zhen, W. Tang, Y. J. Chuang, T. Todd, W. Zhang, X. Lin, G. Niu, G. Liu, L. Wang, Z. Pan, X. Chen and J. Xie, *ACS nano*, 2014, **8**, 6004-6013.
152. T. Araki, K. Ogawara, H. Suzuki, R. Kawai, T. Watanabe, T. Ono and K. Higaki, *J. Controlled Release*, 2015, **200**, 106-114.
153. K. P. Olive, M. A. Jacobetz, C. J. Davidson, A. Gopinathan, D. McIntyre, D. Honess, B. Madhu, M. A. Goldgraben, M. E. Caldwell, D. Allard, K. K. Frese, G. DeNicola, C. Feig, C. Combs, S. P. Winter, H. Ireland-Zecchini, S. Reichelt, W. J. Howat, A. Chang, M. Dhara, L. Wang, F. Rückert, R. Grützmann, C. Pilarsky, K. Izeradjene, S. R. Hingorani, P. Huang, S. E. Davies, W. Plunkett, M. Egorin, R. H. Hruban,

- N. Whitebread, K. McGovern, J. Adams, C. Iacobuzio-Donahue, J. Griffiths and D. A. Tuveson, *Science*, 2009, **324**, 1457-1461.
154. Mara H. Sherman, Ruth T. Yu, Dannielle D. Engle, N. Ding, Annette R. Atkins, H. Tiriatic, Eric A. Collisson, F. Connor, T. Van Dyke, S. Kozlov, P. Martin, Tiffany W. Tseng, David W. Dawson, Timothy R. Donahue, A. Masamune, T. Shimosegawa, Minoti V. Apte, Jeremy S. Wilson, B. Ng, Sue L. Lau, Jenny E. Gunton, Geoffrey M. Wahl, T. Hunter, Jeffrey A. Drebin, Peter J. O'Dwyer, C. Liddle, David A. Tuveson, M. Downes and Ronald M. Evans, *Cell*, 2014, **159**, 80-93.
155. J. P. Celli, N. Solban, A. Liang, S. P. Pereira and T. Hasan, *Lasers Surg. Med.*, 2011, **43**, 565-574.
156. I. Rizvi, J. P. Celli, C. L. Evans, A. O. Abu-Yousif, A. Muzikansky, B. W. Pogue, D. Finkelstein and T. Hasan, *Cancer Res.*, 2010, **70**, 9319-9328.
157. D. A. Bellnier, Y. K. Ho, R. K. Pandey, J. R. Missert and T. J. Dougherty, *Photochem. Photobiol.*, 1989, **50**, 221-228.
158. C. J. Gomer and A. Ferrario, *Cancer Res.*, 1990, **50**, 3985-3990.
159. W.-S. Chan, J. F. Marshall, R. Svensen, J. Bedwell and I. R. Hart, *Cancer Res.*, 1990, **50**, 4533-4538.
160. R. Weijer, M. Broekgaarden, M. Kos, R. Vught, E. A. J. Rauws, T. M. van Gulik, G. Storm and M. Heger, *J. Photochem. Photobiol., C*, 2015, **23**, 103-131.
161. M. J. Bovis, J. H. Woodhams, M. Loizidou, D. Scheglmann, S. G. Bown and A. J. MacRobert, *J Controlled Release*, 2012, **157**, 196-205.
162. J. Buchholz, B. Kaser-Hotz, T. Khan, C. Rohrer Bley, K. Melzer, R. A. Schwendener, M. Roos and H. Walt, *Clin. Cancer Res.*, 2005, **11**, 7538-7544.
163. V. Reshetov, H.-P. Lassalle, A. François, D. Dumas, S. Hupont, S. Gräfe, V. Filipe, W. Jiskoot, F. Guillemin, V. Zorin and L. Bezdetnaya, *Int. J. Nanomed.*, 2013, **8**, 3817-3831.
164. S. A. H. J. de Visscher, S. Kaščáková, H. S. de Bruijn, A. v. d. P. van den Heuvel, A. Amelink, H. J. C. M. Sterenborg, D. J. Robinson, J. L. N. Roodenburg and M. J. H. Witjes, *Lasers Surg. Med.*, 2011, **43**, 528-536.
165. B. Sennino, T. Ishiguro-Oonuma, Y. Wei, R. M. Naylor, C. W. Williamson, V. Bhagwandin, S. P. Tabruyn, W.-K. You, H. A. Chapman, J. G. Christensen, D. T. Aftab and D. M. McDonald, *Cancer Discovery*, 2012, **2**, 270-287.
166. X. Xue and X. J. Liang, *Chin. J. Cancer*, 2012, **31**, 100-109.
167. K. Berg, P. K. Selbo, L. Prasmickaite, T. E. Tjelle, K. Sandvig, J. Moan, G. Gaudernack, O. Fodstad, S. Kjolsrud, H. Anholt, G. H. Rodal, S. K. Rodal and A. Hogset, *Cancer Res.*, 1999, **59**, 1180-1183.
168. K. Berg, A. Dietze, O. Kaalhus and A. Hogset, *Clin. Cancer Res.*, 2005, **11**, 8476-8485.
169. O. J. Norum, J. V. Gaustad, E. Angell-Petersen, E. K. Rofstad, Q. Peng, K. E. Giercksky and K. Berg, *Photochem. Photobiol.*, 2009, **85**, 740-749.
170. <https://clinicaltrials.gov>, NCT00993512.
171. <https://clinicaltrials.gov>, NCT01900158.
172. G. Pasparakis, T. Manouras, M. Vamvakaki and P. Argitis, *Nature communications*, 2014, **5**, 3623.
173. R. L. Elliott, *Surg. Oncol.*, 2012, **21**, 53-55.
174. K. Strebhardt and A. Ullrich, *Nat. Rev. Cancer*, 2008, **8**, 473-480.
175. I. Pastan, M. C. Willingham and D. J. Fitzgerald, *Cell*, 1986, **47**, 641-648.
176. A. Antignani and D. Fitzgerald, *Toxins*, 2013, **5**, 1486-1502.
177. Y. V. Kovtun and V. S. Goldmacher, *Cancer Lett.*, 2007, **255**, 232-240.
178. M. C. Garnett, *Adv. Drug Delivery Rev.*, 2001, **53**, 171-216.
179. B. G. Smaglo, D. Aldeghaither and L. M. Weiner, *Nat. Rev. Clin. Oncol.*, 2014, **11**, 637-648.
180. A. Koshkaryev, R. Sawant, M. Deshpande and V. Torchilin, *Adv. Drug Delivery Rev.*, 2013, **65**, 24-35.
181. R. V. Chari, M. L. Miller and W. C. Widdison, *Angew. Chem., Int. Ed.*, 2014, **53**, 3796-3827.
182. I. Sassoon and V. Blanc, *Methods Mol. Biol.*, 2013, **1045**, 1-27.
183. A. J. Bullous, C. M. Alonso and R. W. Boyle, *Photochemical & photobiological sciences : Official journal of the European Photochemistry Association and the European Society for Photobiology*, 2011, **10**, 721-750.

184. G. A. van Dongen, G. W. Visser and M. B. Vrouenraets, *Adv. Drug Delivery Rev.*, 2004, **56**, 31-52.
185. D. Mew, C. K. Wat, G. H. Towers and J. G. Levy, *J. Immunol.*, 1983, **130**, 1473-1477.
186. C. K. Wat, D. Mew, J. G. Levy and G. H. Towers, *Prog. Clin. Biol. Res.*, 1984, **170**, 351-359.
187. D. Mew, V. Lum, C. K. Wat, G. H. Towers, C. H. Sun, R. J. Walter, W. Wright, M. W. Berns and J. G. Levy, *Cancer Res.*, 1985, **45**, 4380-4386.
188. M. D. Savellano and T. Hasan, *Photochem. Photobiol.*, 2003, **77**, 431-439.
189. M. D. Savellano and T. Hasan, *Clin. Cancer Res.*, 2005, **11**, 1658-1668.
190. A. O. Abu-Yousif, A. C. Moor, X. Zheng, M. D. Savellano, W. Yu, P. K. Selbo and T. Hasan, *Cancer Lett.*, 2012, **321**, 120-127.
191. K. L. Molpus, M. R. Hamblin, I. Rizvi and T. Hasan, *Gynecol. Oncol.*, 2000, **76**, 397-404.
192. N. S. Soukos, M. R. Hamblin, S. Keel, R. L. Fabian, T. F. Deutsch and T. Hasan, *Cancer Res.*, 2001, **61**, 4490-4496.
193. I. Rizvi, T. A. Dinh, W. Yu, Y. Chang, M. E. Sherwood and T. Hasan, *Isr. J. Chem.*, 2012, **52**, 776-787.
194. L. R. Duska, M. R. Hamblin, M. P. Bamberg and T. Hasan, *Br. J. Cancer*, 1997, **75**, 837-844.
195. M. R. Hamblin, J. L. Miller and T. Hasan, *Cancer Res.*, 1996, **56**, 5205-5210.
196. B. A. Goff, M. Bamberg and T. Hasan, *Cancer Res.*, 1991, **51**, 4762-4767.
197. M. Del Governatore, M. R. Hamblin, C. R. Shea, I. Rizvi, K. G. Molpus, K. K. Tanabe and T. Hasan, *Cancer Res.*, 2000, **60**, 4200-4205.
198. B. A. Goff, U. Hermanto, J. Rumbaugh, J. Blake, M. Bamberg and T. Hasan, *Br. J. Cancer*, 1994, **70**, 474-480.
199. A. R. Oseroff, D. Ohuoha, T. Hasan, J. C. Bommer and M. L. Yarmush, *Proc. Natl. Acad. Sci. U. S. A.*, 1986, **83**, 8744-8748.
200. M. R. Hamblin, M. Del Governatore, I. Rizvi and T. Hasan, *Br. J. Cancer*, 2000, **83**, 1544-1551.
201. M. Mitsunaga, M. Ogawa, N. Kosaka, L. T. Rosenblum, P. L. Choyke and H. Kobayashi, *Nat. Med.*, 2011, **17**, 1685-1691.
202. M. B. Vrouenraets, G. W. Visser, M. Stigter, H. Oppelaar, G. B. Snow and G. A. van Dongen, *Cancer Res.*, 2001, **61**, 1970-1975.
203. M. B. Vrouenraets, G. W. Visser, F. A. Stewart, M. Stigter, H. Oppelaar, P. E. Postmus, G. B. Snow and G. A. van Dongen, *Cancer Res.*, 1999, **59**, 1505-1513.
204. A. W. Hemming, N. L. Davis, B. Dubois, N. F. Quenville and R. J. Finley, *Surg. Oncol.*, 1993, **2**, 187-196.
205. S. Schmidt, U. Wagner, B. Schultes, P. Oehr, W. Decler, W. Ertmer, H. Lubaschowski, H. J. Biersack and D. Krebs, *Fortschr. Med.*, 1992, **110**, 298-301.
206. J. P. Celli, B. Q. Spring, I. Rizvi, C. L. Evans, K. S. Samkoe, S. Verma, B. W. Pogue and T. Hasan, *Chem. Rev.*, 2010, **110**, 2795-2838.
207. G. Casi and D. Neri, *J. Controlled Release*, 2012, **161**, 422-428.
208. L. R. Duska, M. R. Hamblin, J. L. Miller and T. Hasan, *J. Natl. Cancer Inst.*, 1999, **91**, 1557-1563.
209. J. Dahle, O. Kaalhus, J. Moan and H. B. Steen, *Proc. Natl. Acad. Sci. U. S. A.*, 1997, **94**, 1773-1778.
210. J. Dahle, E. Angell-Petersen, H. B. Steen and J. Moan, *Photochem. Photobiol.*, 2001, **73**, 378-387.
211. F. Poyer, C. D. Thomas, G. Garcia, A. Croisy, D. Carrez, P. Maillard, M. Lupu and J. Mispelter, *Photodiagn. Photodyn. Ther.*, 2012, **9**, 303-309.
212. I. Postiglione, A. Chiaviello and G. Palumbo, *Cancers*, 2011, **3**, 2597-2629.
213. M. Bhatti, G. Yahiolu, L. R. Milgrom, M. Garcia-Maya, K. A. Chester and M. P. Deonarain, *Int. J. Cancer*, 2008, **122**, 1155-1163.
214. C. Staneloudi, K. A. Smith, R. Hudson, N. Malatesti, H. Savoie, R. W. Boyle and J. Greenman, *Immunology*, 2007, **120**, 512-517.
215. M. K. Kuimova, M. Bhatti, M. Deonarain, G. Yahiolu, J. A. Levitt, I. Stamati, K. Suhling and D. Phillips, *Photochemical & photobiological sciences : Official journal of the European Photochemistry Association and the European Society for Photobiology*, 2007, **6**, 933-939.
216. R. Heukers, P. M. van Bergen en Henegouwen and S. Oliveira, *Nanomedicine*, 2014, **10**, 1441-1451.

217. K. Sato, T. Nagaya, P. L. Choyke and H. Kobayashi, *Theranostics*, 2015, **5**, 698-709.
218. K. Sato, H. Hanaoka, R. Watanabe, T. Nakajima, P. L. Choyke and H. Kobayashi, *Mol. Cancer Ther.*, 2015, **14**, 141-150.
219. <https://clinicaltrials.gov, NCT02422979>.
220. X. Zhao, H. Li and R. J. Lee, *Expert Opin. Drug Delivery*, 2008, **5**, 309-319.
221. K. Temming, R. M. Schiffelers, G. Molema and R. J. Kok, *Drug Resist. Updates*, 2005, **8**, 381-402.
222. A. Quarta, D. Bernareggi, F. Benigni, E. Luison, G. Nano, S. Nitti, M. C. Cesta, L. Di Ciccio, S. Canevari, T. Pellegrino and M. Figini, *Nanoscale*, 2015, **7**, 2336-2351.
223. S. Oliveira, R. Heukers, J. Sornkom, R. J. Kok and P. M. P. van Bergen en Henegouwen, *J. Controlled Release*, 2013, **172**, 607-617.
224. G. Thurston, J. W. McLean, M. Rizen, P. Baluk, A. Haskell, T. J. Murphy, D. Hanahan and D. M. McDonald, *J. Clin. Invest.*, 1998, **101**, 1401-1413.
225. R. B. Campbell, B. Ying, G. M. Kuesters and R. Hemphill, *J. Pharm. Sci.*, 2009, **98**, 411-429.
226. A. Abu Lila, T. Ishida and H. Kiwada, *Pharm. Res.*, 2009, **27**, 1171-1183.
227. E. Bilensoy, *Expert Opin. Drug Delivery*, 2010, **7**, 795-809.
228. T. Stuchinskaya, M. Moreno, M. J. Cook, D. R. Edwards and D. A. Russell, *Photochemical & photobiological sciences : Official journal of the European Photochemistry Association and the European Society for Photobiology*, 2011, **10**, 822-831.
229. G. Obaid, I. Chambrier, M. J. Cook and D. A. Russell, *Angew. Chem., Int. Ed.*, 2012, **51**, 6158-6162.
230. J. D. Meyers, Y. Cheng, A.-M. Broome, R. S. Agnes, M. D. Schluchter, S. Margevicius, X. Wang, M. E. Kenney, C. Burda and J. P. Basilion, *Particle & particle systems characterization : measurement and description of particle properties and behavior in powders and other disperse systems*, 2015, **32**, 448-457.
231. M. Gary-Bobo, Y. Mir, C. Rouxel, D. Brevet, I. Basile, M. Maynadier, O. Vaillant, O. Mongin, M. Blanchard-Desce, A. Morère, M. Garcia, J.-O. Durand and L. Raehm, *Angew. Chem., Int. Ed.*, 2011, **50**, 11425-11429.
232. G. R. Reddy, M. S. Bhojani, P. McConville, J. Moody, B. A. Moffat, D. E. Hall, G. Kim, Y. E. Koo, M. J. Woolliscroft, J. V. Sugai, T. D. Johnson, M. A. Philbert, R. Kopelman, A. Rehemtulla and B. D. Ross, *Clin. Cancer Res.*, 2006, **12**, 6677-6686.
233. C. S. Jin, L. Cui, F. Wang, J. Chen and G. Zheng, *Adv. Healthcare Mater.*, 2014, **3**, 1240-1249.
234. A. Gijssens, A. Derycke, L. Missiaen, D. De Vos, J. Huwyler, A. Eberle and P. de Witte, *Int. J. Cancer*, 2002, **101**, 78-85.
235. L. C. Bergstrom, I. Vucenik, I. K. Hagen, S. A. Chernomorsky and R. D. Poretz, *J. Photochem. Photobiol., B*, 1994, **24**, 17-23.
236. Y. Mir, S. A. Elrington and T. Hasan, *Nanomedicine*, 2013, **9**, 1114-1122.
237. K. Ichikawa, T. Hikita, N. Maeda, S. Yonezawa, Y. Takeuchi, T. Asai, Y. Namba and N. Oku, *Biochim. Biophys. Acta, Biomembr.*, 2005, **1669**, 69-74.
238. H. Benachour, A. Sève, T. Bastogne, C. Frochot, R. Vanderesse, J. Jasniewski, I. Miladi, C. Billotey, O. Tillement, F. Lux and M. Barberi-Heyob, *Theranostics*, 2012, **2**, 889-904.
239. G. R. Reddy, M. S. Bhojani, P. McConville, J. Moody, B. A. Moffat, D. E. Hall, G. Kim, Y.-E. L. Koo, M. J. Woolliscroft, J. V. Sugai, T. D. Johnson, M. A. Philbert, R. Kopelman, A. Rehemtulla and B. D. Ross, *Clin. Cancer Res.*, 2006, **12**, 6677-6686.
240. C. Edmonds, S. Hagan, S. M. Gallagher-Colombo, T. M. Busch and K. A. Cengel, *Cancer Biol. Ther.*, 2012, **13**, 1463-1470.
241. N. Solban, P. K. Selbo, A. K. Sinha, S. K. Chang and T. Hasan, *Cancer Res.*, 2006, **66**, 5633-5640.
242. A. Ferrario, K. Von Tiehl, S. Wong, M. Luna and C. J. Gomer, *Cancer Res.*, 2002, **62**, 3956-3961.
243. S. Hatz, L. Poulsen and P. R. Ogilby, *Photochem. Photobiol.*, 2008, **84**, 1284-1290.
244. A. Garg, D. Nowis, J. Golab and P. Agostinis, *Apoptosis*, 2010, **15**, 1050-1071.
245. D. Kessel and M. Castelli, *Photochem. Photobiol.*, 2001, **74**, 318-322.
246. E. Buytaert, M. Dewaele and P. Agostinis, *Biochim. Biophys. Acta*, 2007, **1776**, 86-107.

247. M. Broekgaarden, R. Weijer, T. M. van Gulik, M. R. Hamblin and M. Heger, *Cancer Metastasis Rev.*, 2015, **34**, 643-690.
248. J. Moan, K. Berg, H. Anholt and K. Madslie, *Int. J. Cancer*, 1994, **58**, 865-870.
249. P. D. Wilson, R. A. Firestone and J. Lenard, *J. Cell Biol.*, 1987, **104**, 1223-1229.
250. S. Anand, C. Wilson, T. Hasan and E. V. Maytin, *Cancer Res.*, 2011, **71**, 6040-6050.
251. S. Anand, K. R. Rollakanti, R. L. Horst, T. Hasan and E. V. Maytin, *Photochem. Photobiol.*, 2014, **90**, 1126-1135.
252. S. Anand, T. Hasan and E. V. Maytin, *Mol. Cancer Ther.*, 2013, **12**, 1638-1650.
253. A. K. Sinha, S. Anand, B. J. Ortel, Y. Chang, Z. Mai, T. Hasan and E. V. Maytin, *Br. J. Cancer*, 2006, **95**, 485-495.
254. D. Nowis, M. Legat, T. Grzela, J. Niderla, E. Wilczek, G. M. Wilczynski, E. Glodkowska, P. Mrowka, T. Issat and J. Dulak, *Oncogene*, 2006, **25**, 3365-3374.
255. S. G. Kimani, J. B. Phillips, J. I. Bruce, A. J. MacRobert and J. P. Golding, *Photochem. Photobiol.*, 2012, **88**, 175-187.
256. G. L. Semenza, *Nat. Rev. Cancer*, 2003, **3**, 721-732.
257. A. Ferrario and C. Gomer, *J. Environ. Pathol., Toxicol. Oncol.*, 2006, **25**, 251-260.
258. A. Ferrario, S. Lim, F. Xu, M. Luna, K. J. Gaffney, N. A. Petasis, A. H. Schönthal and C. J. Gomer, *Cancer Lett.*, 2011, **304**, 33-40.
259. M. Broekgaarden, R. Weijer, M. Krekorian, B. van den IJssel, M. Kos, L. K. Alles, A. C. van Wijk, Z. Bikadi, E. Hazai, T. M. van Gulik and M. Heger, *Nano Res.*, 2015, **16**, 19960-19977.
260. R. Weijer, M. Broekgaarden, M. Krekorian, L. K. Alles, A. C. van Wijk, C. Mackaaij, J. Verheij, A. C. van der Wal, T. M. van Gulik, G. Storm and M. Heger, *Oncotarget*, 2015, **7**, 3341-3356.
261. A. Ferrario, K. F. von Tiehl, N. Rucker, M. A. Schwarz, P. S. Gill and C. J. Gomer, *Cancer Res.*, 2000, **60**, 4066-4069.
262. P. A. Tsytler, M. C. O'Flaherty, D. V. Sakharov, J. Krijgsveld and M. R. Egmond, *J. Proteome Res.*, 2008, **7**, 3868-3878.
263. A. Szokalska, M. Makowski, D. Nowis, G. M. Wilczynski, M. Kujawa, C. Wójcik, I. Mlynarczuk-Bialy, P. Salwa, J. Bil, S. Janowska, P. Agostinis, T. Verfaillie, M. Bugajski, J. Gietka, T. Issat, E. Glodkowska, P. Mrówka, T. Stoklosa, M. R. Hamblin, P. Mróz, M. Jakóbsiak and J. Golab, *Cancer Res.*, 2009, **69**, 4235-4243.
264. A. Ferrario and C. J. Gomer, *Cancer Lett.*, 2010, **289**, 188-194.
265. M. Nonaka, H. Ikeda and T. Inokuchi, *Photochem. Photobiol.*, 2004, **79**, 94-98.
266. I. Coupienne, S. b. Bontems, M. Dewaele, N. Rubio, Y. Habraken, S. Fulda, P. Agostinis and J. Piette, *Biochem. Pharmacol.*, 2011, **81**, 606-616.
267. H. M. Chen, C. M. Liu, H. Yang, H. Y. Chou, C. P. Chiang and M. Y. Kuo, *J. Oral Pathol. Med.*, 2011, **40**, 483-489.
268. M. Broekgaarden, M. Kos, F. A. Jurg, A. A. van Beek, T. M. van Gulik and M. Heger, *Int. J. Mol. Sci.*, 2015, **16**, 19960-19977.
269. J. Bartek and J. Lukas, *Curr. Opin. Cell Biol.*, 2007, **19**, 238-245.
270. B. Vogelstein, D. Lane and A. J. Levine, *Nature*, 2000, **408**, 307-310.
271. D. Kessel, *Photochem. Photobiol.*, 2014, **90**, 1211-1213.
272. B. Q. Spring, I. Rizvi, N. Xu and T. Hasan, *Photochemical & photobiological sciences : Official journal of the European Photochemistry Association and the European Society for Photobiology*, 2015, **14**, 1476-1491.
273. M. Nonaka, H. Ikeda and T. Inokuchi, *Cancer Lett.*, 2002, **184**, 171-178.
274. P. Baas, I. P. van Geel, H. Oppelaar, M. Meyer, J. H. Beynen, N. van Zandwijk and F. A. Stewart, *Br. J. Cancer*, 1996, **73**, 945-951.
275. P. M. LoRusso, R. Canetta, J. A. Wagner, E. P. Balogh, S. J. Nass, S. A. Boerner and J. Hohnaker, *Clin. Cancer Res.*, 2012, **18**, 6101-6109.
276. H. Zhang, G. Wang and H. Yang, *Expert Opin. Drug Delivery*, 2011, **8**, 171-190.

277. A. K. Iyer, A. Singh, S. Ganta and M. M. Amiji, *Adv. Drug Delivery Rev.*, 2013, **65**, 1784-1802.
278. C. M. Hu, S. Aryal and L. Zhang, *Ther. Delivery*, 2010, **1**, 323-334.
279. A. J. Mieszawska, A. Gianella, D. P. Cormode, Y. Zhao, A. Meijerink, R. Langer, O. C. Farokhzad, Z. A. Fayad and W. J. Mulder, *Chem. Commun. (Cambridge, U. K.)*, 2012, **48**, 5835-5837.
280. S. Tangutoori, B. Q. Spring, Z. Mai, A. Palanisami, L. Mensah and T. Hasan, *Nanomedicine*, 2015, DOI: 10.1016/j.nano.2015.08.007.
281. C. He, D. Liu and W. Lin, *ACS nano*, 2015, **9**, 991-1003.
282. Y. Li, T. Y. Lin, Y. Luo, Q. Liu, W. Xiao, W. Guo, D. Lac, H. Zhang, C. Feng, S. Wachsmann-Hogiu, J. H. Walton, S. R. Cherry, D. J. Rowland, D. Kukis, C. Pan and K. S. Lam, *Nature communications*, 2014, **5**, 4712.
283. J. F. Lovell, C. S. Jin, E. Huynh, T. D. MacDonald, W. Cao and G. Zheng, *Angew. Chem., Int. Ed.*, 2012, **51**, 2429-2433.
284. K. A. Carter, S. Shao, M. I. Hoopes, D. Luo, B. Ahsan, V. M. Grigoryants, W. Song, H. Huang, G. Zhang, R. K. Pandey, J. Geng, B. A. Pfeifer, C. P. Scholes, J. Ortega, M. Karttunen and J. F. Lovell, *Nature communications*, 2014, **5**, 3546.
285. W. Wang, Y. Wen, L. Xu, H. Du, Y. Zhou and X. Zhang, *Chemistry*, 2014, **20**, 7796-7802.
286. B. Chen, B. W. Pogue, P. J. Hoopes and T. Hasan, *Crit. Rev. Eukaryotic Gene Expression*, 2006, **16**, 279-305.
287. B. Chen, B. W. Pogue, P. J. Hoopes and T. Hasan, *Int. J. Radiat. Oncol., Biol., Phys.*, 2005, **61**, 1216-1226.
288. B. Chen, B. W. Pogue, I. A. Goodwin, J. A. O'Hara, C. M. Wilmot, J. E. Hutchins, P. J. Hoopes and T. Hasan, *Radiat. Res.*, 2003, **160**, 452-459.
289. V. H. Fingar, P. K. Kik, P. S. Haydon, P. B. Cerrito, M. Tseng, E. Abang and T. J. Wieman, *Br. J. Cancer*, 1999, **79**, 1702-1708.
290. U. Schmidt-Erfurth and T. Hasan, *Surv. Ophthalmol.*, 2000, **45**, 195-214.
291. M. Kramer, J. W. Miller, N. Michaud, R. S. Moulton, T. Hasan, T. J. Flotte and E. S. Gragoudas, *Ophthalmology*, 1996, **103**, 427-438.
292. J. Trachtenberg, A. Bogaards, R. A. Weersink, M. A. Haider, A. Evans, S. A. McCluskey, A. Scherz, M. R. Gertner, C. Yue, S. Appu, A. Aprikian, J. Savard, B. C. Wilson and M. Elhilali, *J. Urol.*, 2007, **178**, 1974-1979; discussion 1979.
293. B. Pegaz, E. Debeve, F. Borle, J. P. Ballini, H. van den Bergh and Y. N. Kouakou-Konan, *J. Photochem. Photobiol., B*, 2005, **80**, 19-27.
294. B. Pegaz, E. Debeve, J. P. Ballini, Y. N. Konan-Kouakou and H. van den Bergh, *J. Photochem. Photobiol., B*, 2006, **85**, 216-222.
295. D. Neri and R. Bicknell, *Nat. Rev. Cancer*, 2005, **5**, 436-446.
296. M. Garcia-Diaz, M. Kawakubo, P. Mroz, M. L. Sagrista, M. Mora, S. Nonell and M. R. Hamblin, *J. Controlled Release*, 2012, **162**, 355-363.
297. M. Camerin, M. Magaraggia, M. Soncin, G. Jori, M. Moreno, I. Chambrier, M. J. Cook and D. A. Russell, *European journal of cancer*, 2010, **46**, 1910-1918.
298. D. Bechet, F. Auger, P. Couleaud, E. Marty, L. Ravasi, N. Durieux, C. Bonnet, F. Plenat, C. Frochot, S. Mordon, O. Tillement, R. Vanderesse, F. Lux, P. Perriat, F. Guillemin and M. Barberi-Heyob, *Nanomedicine*, 2015, **11**, 657-670.
299. P. Couleaud, D. Bechet, R. Vanderesse, M. Barberi-Heyob, A. C. Faure, S. Roux, O. Tillement, S. Porhel, F. Guillemin and C. Frochot, *Nanomedicine (London, U. K.)*, 2011, **6**, 995-1009.
300. N. Thomas, D. Bechet, P. Becuwe, L. Tirand, R. Vanderesse, C. Frochot, F. Guillemin and M. Barberi-Heyob, *J. Photochem. Photobiol., B*, 2009, **96**, 101-108.
301. N. Thomas, L. Tirand, E. Chatelut, F. Plenat, C. Frochot, M. Dodeller, F. Guillemin and M. Barberi-Heyob, *Photochemical & photobiological sciences : Official journal of the European Photochemistry Association and the European Society for Photobiology*, 2008, **7**, 433-441.

